ISTANBUL TECHNICAL UNIVERSITY ★ GRADUATE SCHOOL

MODAL BALANCING OF FLEXIBLE ROTORS WITH GYROSCOPIC EFFECTS USING KALMAN FILTER

M.Sc. THESIS

Canberk NAMIK

Department of Mechanical Engineering

Machine Dynamics, Vibration and Acoustics Programme

OCTOBER 2023

ISTANBUL TECHNICAL UNIVERSITY ★ GRADUATE SCHOOL

MODAL BALANCING OF FLEXIBLE ROTORS WITH GYROSCOPIC EFFECTS USING KALMAN FILTER

M.Sc. THESIS

Canberk NAMIK
(503201405)

Department of Mechanical Engineering

Machine Dynamics, Vibration and Acoustics Programme

Thesis Advisor: Prof. Dr. Haluk EROL

OCTOBER 2023

İSTANBUL TEKNİK ÜNİVERSİTESİ ★ LİSANSÜSTÜ EĞİTİM ENSTİTÜSÜ

JİROSKOPİK ETKİ ALTINDAKİ ESNEK ROTORLARIN KALMAN FİLTRESİ İLE MODAL DENGELENMESİ

Yüksek Lisans Tezi

Canberk NAMIK
(503201405)

Makine Mühendisliği Anabilim Dalı

Makine Dinamiği, Titreşim ve Akustik Programı

Tez Danışmanı: Prof. Dr. Haluk EROL

EKİM 2023

Canberk Namık, a M.Sc. student of İTU Graduate School student ID 503201405, successfully defended the thesis entitled “MODAL BALANCING OF FLEXIBLE ROTORS WITH GYROSCOPIC EFFECTS USING KALMAN FILTER” which he prepared after fulfilling the requirements specified in the associated legislations, before the jury whose signatures are below.

Thesis Advisor :	**Prof. Dr. Haluk EROL** İstanbul Technical University	……
Jury Members :	**Prof. Dr. Ata MUĞAN** İstanbul Technical University	……
	Prof. Dr. Orhan ÇAKAR Fırat University	……

Date of Submission : 26 May 2023
Date of Defense : 9 October 2023

To my family,

FOREWORD

Considering the wide usage of rotating machinery in industry, one topic that is proven to be very important is the mass balancing of the rotating hardware. Looking at the vibrations' perspective; depending on the rotors operating speed being whether above or below its first critical speed, the balancing approach to be used changes. When it is below the first critical speed, rigid balancing approaches are used which is well-known theoretically and practically. If the operating speed is beyond first critical speed, then flexible balancing should be used. There is not a settled approach for flexible balancing and applications may vary. Some of them include very radical assumptions and some of them are fully experimental. In this study, we will try to provide a robust and precise solution to the flexible balancing issue.

I am grateful to my thesis supervisor Prof. Dr. Haluk Erol for guiding me during the whole study and sharing his valuable experiences and knowledge with me through our study. I also would like to thank dear Umut Karahan and Mucahit Dilekcan who are employees of TEI-TUSAS Engine Industries Inc. for supporting us on the usage of their test facility.

I dedicate this thesis to my family who has always been supporting me through my entire life.

October 2023

Canberk NAMIK

Mechanical Engineer

TABLE OF CONTENTS

ABBREVIATIONS

FE **:** Finite Element

CoG **:** Centre of Gravity

FEM **:** Finite Element Method

1D **:** One Dimensional

FRF **:** Frequency Response Function

DoF **:** Degree of Freedom

SYMBOLS

$\boldsymbol{m}$	**:** Mass
$\boldsymbol{c}$	**:** Damping
$\boldsymbol{k}$	**:** Stiffness
$\boldsymbol{x, y, z, r}$	**:** Displacement components
$\boldsymbol{\dot{x}, \dot{y}, \dot{z}, \dot{r}}$	**:** Velocity components
$\boldsymbol{\ddot{x}, \ddot{y}, \ddot{z}, \ddot{r}}$	**:** Acceleration components
$\boldsymbol{a}$	**:** Mass eccentricity
$\boldsymbol{\omega}$	**:** Angular velocity
$\boldsymbol{\zeta}$	**:** Damping ratio
$\boldsymbol{\omega_n}$	**:** Natural frequency
$\boldsymbol{\lambda}$	**:** Eigenvalue
$\boldsymbol{M_x, M_y, M_z}$	**:** Moment components
$\boldsymbol{I_t}$	**:** Transverse moment of inertia
$\boldsymbol{I_p}$	**:** Polar moment of inertia
$\boldsymbol{\dot{\omega}}$	**:** Angular acceleration
$\boldsymbol{\theta_x, \theta_y, \theta_z}$	**:** Angular displacement components
$\boldsymbol{\dot{\theta}_x, \dot{\theta}_y, \dot{\theta}_z}$	**:** Angular velocity components
$\boldsymbol{\ddot{\theta}_x, \ddot{\theta}_y, \ddot{\theta}_z}$	**:** Angular acceleration components
$\boldsymbol{\phi}$	**:** Mode shape
$[\boldsymbol{M}]$	**:** Mass matrix
$[\boldsymbol{C}]$	**:** Damping matrix
$[\boldsymbol{K}]$	**:** Stiffness matrix
$[\boldsymbol{G}(\boldsymbol{\omega})]$	**:** Gyroscopic matrix
$\{\boldsymbol{x}\}, \{\dot{\boldsymbol{x}}\}, \{\ddot{\boldsymbol{x}}\}$	**:** Displacement, velocity, acceleration vectors
$\{\boldsymbol{f}(\boldsymbol{t})\}$	**:** Excitation vector
$\boldsymbol{\rho}$	**:** Density
$\boldsymbol{A}$	**:** Section area

ℓ : Length

E : Modulus of elasticity

I : Second moment of inertia

U : Unbalance

φ : Unbalance phase angle

LIST OF TABLES

Pages

LIST OF FIGURES

Pages

MODAL BALANCING OF FLEXIBLE ROTORS WITH GYROSCOPIC EFFECTS USING KALMAN FILTER

SUMMARY

At present day, rotating machinery is being used at numerous different fields. Looking to its development so far, demand from the rotating components is evolving towards becoming lighter and spinning faster by still keeping the same or higher amount of life cycles. The mentioned trend makes rotating components less stiff and increases their operating speed range. This can possibly introduce vibration driven problems such as noise, excessive wear or shortened fatigue life. One topic related with vibrations is the balancing of the rotating hardware. Balancing approach of rotating components differ depending on the classification of a rotor being "rigid" or "flexible". The difference between the two is, a rigid rotor operates significantly less than its first critical bending speed and a flexible rotor operates close to or above its first critical bending speed. Balancing of rigid rotors are very well-known theoretically and practically. On the other hand, flexible rotor balancing is not standardized and there are various approaches for the process.

This study will try to develop a robust and precise flexible balancing procedure considering the gyroscopic effect which is usually neglected at many flexible balancing techniques. The developed approach will be suitable for both test rig and in-site balancing. The approach hosts a FE model to be used and does not require any trial mass. It is necessary to collect displacement data from the rotating hardware at close to critical speeds. FE model and sensor data are adequate to generate the unbalance values and positions using a series of calculations. These calculations require a force reconstruction method to be used and it is decided to use Augmented Kalman Filter. A regular Augmented Kalman Filter is not suitable for capturing the desired phenomena's, thus, some additional tweaks are made so that it fits better for the nature of rotordynamics. When the forces are generated, it is an easy effort to obtain unbalance masses and positions. The balancing can be done at close to critical speeds, mode by mode using modal approach and without upsetting the previously balanced modes. An important point on setting the balancing criteria is using the complex eigenvalue analysis to obtain modal properties due to existence of gyroscopic effect.

JİROSKOPİK ETKİ ALTINDAKİ ESNEK ROTORLARIN KALMAN FİLTRESİ İLE MODAL DENGELENMESİ

ÖZET

Günümüzde dönen makineler sayısız farklı alanda kullanılmaktadır. Dönen makinelerin evrildiği yöne bakıldığında; talebin, daha hafif ve daha yüksek dönme hızlarına sahip olup hedeflenen yorulma çevrimi sayısının benzer veya daha da yüksek olması yönünde olduğu göze çarpmaktadır. Bahsedilen bu yönelim, dönen makinelerin rijitliğinin azalmasına ve çalışma hızı bölgesinin genişlemesine sebep olmaktadır. Bu sebeple sistemlerde muhtemel olarak titreşim kaynaklı olmak üzere; gürültü, aşınma, veya çalışma ömründe azalma gibi sorunlar ortaya çıkmaktadır. Bununla beraber, titreşimle doğrudan doğruya ilintili olan bir konu ise dönen makinelerin dengelenmesidir. Dönen makinelerin, veya rotorların, dengelenmesi bu rotorun rijit veya esnek rotor olarak sınıflandırılmasına göre değişmektedir. Esnek ve rijit rotorların arasındaki fark, rijit rotorların ilk kritik hızlarının ilk kritik hızlarının oldukça altında çalışması ve esnek rotorların ise ilk kritik hızlarına yakın veya üzerinde çalışıyor olmasıdır. Rijit rotorların dengelenmesi işlemi teorik olarak gayet iyi bilinen ve standardize edilmiş bir proses olmasına rağmen esnek rotorların dengelenmesi standardize edilmemiştir ve bu problemin çözümü için farklı yöntemler ortaya atılmıştır.

Bu tezde jiroskopik etkinin hesaba katıldığı durumda esnek dengeleme yapabilmek adına güçlü ve hassas bir prosedür geliştirmek amaçlanmıştır. Geliştirilen yaklaşım hem test düzeneği üzerinde hem de çalışma ortamında dengelemeyi gerçekleştirmeye uygun olacaktır.

Tez kapsamında geliştirilmeye çalışılan bu yaklaşım; bünyesinde, bir sonlu eleman modeli oluşturulması ve deneme kütlesi kullanılmaması prensibini barındırmaktadır. Sonlu eleman modelinin kurulması için tek boyutlu kiriş modellerinin kullanılması uygun görülmüştür. Kiriş modellerinin formülasyonu için Euler-Bernoulli ve Timoshenko kirişleri kullanılmış ve bazı noktalarda ise endüstride yaygın olarak kullanılan ticari paket programlara başvurulmuştur.

Çalışma sonucunda önerilen dengeleme yaklaşımına göre rotorlardan ölçüm yoluyla deplasman verilerinin elde edilmesi gerekmektedir. Elde edilecek deplasman verisi ve oluşturulan sonlu eleman modeli, sistem üzerindeki dengesizlik değerlerinin ve konumlarının elde edilebilmesi için gerekli ve yeterli girdilerdir. Deplasman verileri birbirine doksan derecelik konumlandırılmış sensörlerden elde edilebilmektedir ve bir rotor üzerinden birden çok noktadan ölçüm alınması gerekmektedir. Ölçüm sayısı belirli bir alt değerle sınırlandırılmamış olup, ölçüm sayısı arttıkça bu metodun isabetliliği ve tutarlılığı artacaktır.

Bahsi geçen dengeleme işlemini gerçekleştirebilmek için ise bir dizi hesaplama yapmak gereklidir. Bu çalışma kapsamında açıklanan yaklaşımın merkezinde dengesizlik kuvvetlerinin isabetli bir şekilde oluşturulabilmesi için Kalman Filtresi yönteminin kullanılması yatmaktadır. Kalman Filtresi'nin birden çok formülasyonu ve yaklaşımı bulunmaktadır. Dengesizlik kuvvetlerinin oluşturulabilmesi adına Augmented Kalman Filtresi yöntemi kullanılmış ve çözümlemenin rotor dinamiği problemine uygunluğunun arttırılması adına formülasyonda bazı değişiklikler yapılmıştır. Bu değişiklikler, hesaplamalar esnasında çözümün doğru sonuca yakınsaması adına hayati öneme sahiptir. Değişikliklere bakıldığında ise literatürde zaman zaman karşılaşılabilen bir durum olan, Augmented Kalman Filtresinde sistem durumlarından birinin kuvvet yerine dengesizlik olarak formülize edilmesi yatmaktadır. Buna ögre, Kalman Filtresi'nin her zaman adımında değişen bir değeri ön görmeye çalışmasının yerine her zaman sabit olan bir değeri ön görmeye çalışmasının sağlanması hedeflenmiştir.

Çalışma kapsamında, Augmented Kalman Filtresi yöntemiyle elde edilmiş dengesizlik değerleri modal dengeleme yaklaşımına göre ortaya atılmış bazı dengeleme kriterlerine beslenmektedir. Bu dengeleme kriterleri; literatürde yaygınca kullanılan yaklaşımların aksine, jiroskopik etkiyi de göz önünde bulundurmaktadır. Genelleştirmek istendiği takdirde; mevcut literatüre göre dengelemenin, mod şekillerinin hızdan bağımsız olduğu koşullarda mod, mod yapıldığı fakat bu çalışma kapsamında ise hıza bağımlı olarak mod, mod değil kritik hız noktalarında yapılması gerektiği vurgulanmıştır.

Prosedürel olarak yaklaşıldığında, dengesizlik değerleri kritik hızlara yakın hızlarda elde edilip dengeleme işlemi modal yaklaşım ile yapılabilmektedir ve önceki dengelenmiş modların da bozulmaması da sağlanabilinmektedir. Bu bağlamda, rotorun çalışmakta olduğu hız bölgesindeki tüm modların dengelenmesi teorik olarak mümkündür.

Jiroskopik etki göz önünde bulundurularak ve tez kapsamındaki hesaplara dahil edilerek, daha öncesinde bahsedilmiş olan güçlü ve hassas bir metodun geliştirilmesi hedeflenmiştir. Bu sayede ileri ve geri dolanım hareketlerinin dengelenmesi mümkün olmaktadır ve özellikle yüksek hızlarda ortaya çıkacak, esnek dengeleme konusundaki belirsizliğin önüne geçilmek hedeflenmiştir.

Tez çalışmasının ana hedefi geliştirilmiş olan dengeleme formülasyonunun ve yaklaşımının deneysel verilerle desteklenmesi ve doğrulanmasıdır. Bu bağlamda yapılan ilk çalışma ise fiziksel çalışmalar yapılmadan önce nümerik hesaplar yardımıyla bahsi geçen yaklaşımın doğruluğunun tartılmasıdır. Bu hedef doğrultusunda, bir dengesiz rotor-disk problemi kurulmuştur. Kiriş formülasyonları vasıtasıyla, daha önce bahsedildiği üzere, bir sonlu eleman modeli kurulmuştur. Bir test senaryosu belirlenerek, Newmark Algoritması yardımıyla senaryo çerçevesinde hesaplar yapılmış ve problemin zaman uzayındaki çözümü elde edilmiştir. Zaman uzayındaki çözüm üzerinden rastgele seçilmiş birkaç düğüm noktasının verisi Augmented Kalman Fitresine beslenerek, dengesizlik kuvvetleri elde edilmiştir. Sonuç olarak, geliştirilen yaklaşımın nümerik bir problemi çözebilecek kapasiteye sahip olduğu anlaşılmıştır.

Bahsedildiği üzere tez çalışmasının ana hedefinin; dengeleme yaklaşımın deneysel verilerle doğrulanması olup, nümerik sonuçlarda elde edilen başarıdan yola çıkarak

sonraki aşamada testler yapılması uygun görülmüştür. Testler için, dengeleme amacı ile tasarlanmış bir test düzeneği kullanılmıştır. Test düzeneği yataklanmış bir rotor-disk sitemidir ve belirli noktalarında Eddy probları barındırmaktadır. Eddy problarından elde edilen deplasman verileri, ticari yazılımlar vasıtasıyla formülize edilen sistem matrisleriyle beraber Augmented Kalman Filtresine beslenmiştir. Buradan yola çıkarak, iteratif bir süreç ile dengesizlik değerleri elde edilmiş ve dengeleme operasyonu nümerik hesaplar üzerinden yapılmaya çalışılmıştır. Sonuçlara bakıldığında ise, yalnızca ilk mod özelinde yapılan bu çalışmanın ümit vadedici sonuçlar elde ettiği gözlenmiştir.

Tez kapsamında yapılan tüm çalışmalar bir araya getirildiğinde sonuç olarak, Augmented Kalman Filtresi kullanımıyla basit dengleme problemlerinin hem nümerik olarak hem de deneysel olarak demonstrasyonu yapılmıştır. Yapılan hesaplara göre geliştirilen prosedür ümit vadedicidir ve üzerine ek çalışmalar yapılması adına değerli görülmektedir. Bu ek çalışmalara örnek olarak yüksek modların da dengelenmesi örnek olabilmektedir. Ayrıca, Kalman Filtresi formülasyonunda yapılacak bazı değişiklikler vasıtasıyla modal yaklaşım yerine doğrudan yaklaşımın formülize edilebileceği ön görülmektedir. Bu sayede gerçek problemlerde sıklıkla karışılabilen, modlarından birbirinden yeterince ayrışmadığı durumlara çözüm üretilmesinin mümkün olabileceği düşünülmektedir.

1. INTRODUCTION

At present day, rotating machinery is being used in numerous different fields. Looking at its development so far, demand from the rotating components is evolving towards becoming lighter and spinning faster by still keeping the same or higher amount of life cycles. This puts newer weight on engineers' shoulders in areas such as material science or manufacturing technologies. One another area that is affected by this trend is vibration topics. The mentioned trend makes rotating components less stiff and increases their operating speed range. This can possibly introduce problems such as noise, excessive wear or shortened fatigue life.

There are different sources of vibration on rotating hardware depending on the field of application. Some examples can be given as; unbalance, flow-induced vibrations, blade passes or combustion forces. The main motivation of this study will be canceling out the unbalance forces. After the manufacturing of a part, there is always an amount of residue mass unbalance; i.e., the CoG of a part not being coincident with its geometrical center. This is experienced due to many factors, such as manufacturing precision, material non-homogeneity or gravity. In order to avoid unwanted effects, the part has to be balanced after manufacturing. Otherwise, as the mentioned parts are rotating; an unwanted centrifugal force will be introduced on the system, causing noise, wear or lessened high cycle fatigue life.

The balancing approach of rotating components differs depending on the classification of a rotor as "rigid" or "flexible." The difference between the two is a rigid rotor operates significantly less than its first critical bending speed and a flexible rotor operates close to or above its first critical bending speed. Balancing of rigid rotors is very well-known theoretically and practically. It is also standardized, economical and does not require specific operator skills. Rigid rotor balancing consists of two steps as: static and dynamic balancing. On the other hand, flexible rotor balancing is not standardized and there are various approaches for the process. These different

approaches are based on a theoretical approach, a practical approach and a composition of those. Most of the solutions widely used today have errors, such as making very radical assumptions or making multiple trial-error runs with the rotor, which limits the balancing process to be not so precise and becomes very uneconomical and slow. A new approach without neglecting the nature of the rotordynamics and including more physical phenomena by also keeping the balancing process quick, precise and economical would be what the industry demands for the time being.

1.1 Literature Survey

Before developing a new and unique balancing approach, it is a must to understand studies that are already known. For this purpose, it makes sense to focus on some topics, such as rotordynamics and balancing, as these will be the main driving forces of the balancing approach introduced here.

The first area to be highlighted is rotordynamics, which focuses on vibration-induced problems in rotating machinery and tries to develop techniques to lessen the vibration. In this manner, areas such as; the design of rotating machinery, setting convenient operating conditions as well as developing appropriate maintenance techniques are studied. Vibration is tried to be reduced by looking at the source of excitation, mechanism of excitation or natural frequencies of vibration modes [1].

There are different types of excitations in rotating machinery, such as; bending vibrations, torsional vibrations, longitudinal vibrations and vibrations of the rotating structure. For the bending vibrations, the rotating shaft whirls in its rotational plane while keeping the flexural mode that changes throughout the axial length [1]. Bending vibrations are the main point of interest in this study. Torsional vibrations are when the displacement happens to be movement of twisting along the rotational axis. Longitudinal vibrations are deflections of the shaft along the axial direction. Vibrations of rotating structures usually contribute to the bending vibrations by three-dimensional coupling effects. These effects are also studied in this study.

Throughout history, many researchers contributed to rotordynamics. The first paper published on rotordynamics belongs to William John Macquorn Rankine (182-1872), who was a professor at the University of Glasgow. Although he is famous for his work

on the Rankine cycle, which is related to heat engines, he wrote a paper called “On the Centrifugal Force of Rotating Shafts” in 1869. He suggested that centrifugal whirling is impossible beyond a certain speed and defined a limiting length. He also proposed a formula for calculating this certain speed. The definition of “critical speed” was done by Dunkerley in 1894. The basic theory for rotordynamics was published by H. H. Jeffcott in 1919. He used a disk, which is placed in the middle of a shaft, to make some derivations. His model is usually called by his name as “Jeffcott Rotor” [2].

One of the most important explanations is done by Wilfred Campbell (1884-1924). During his work, he often used frequency versus rotational speed plots. These plots were later named after his name as, “Campbell Diagram” [2]. An example Campbell Diagram can be seen in Figure 1.1.

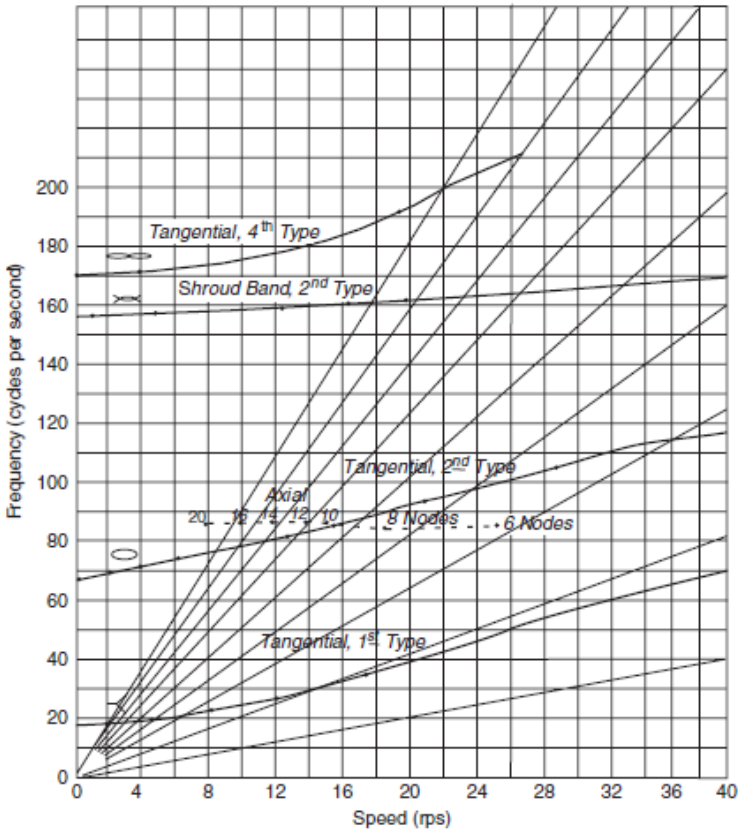

Figure 1.1: Example Campbell Diagram [2].

R.E.D Bishop released some papers in the 1950s and 1960s with some other researchers. These papers made some suggestions related to the unbalance response of continuous rotors, balancing and gyroscopic effect. A summary chart for the historical development of rotordynamics can be seen in Figure 1.2.

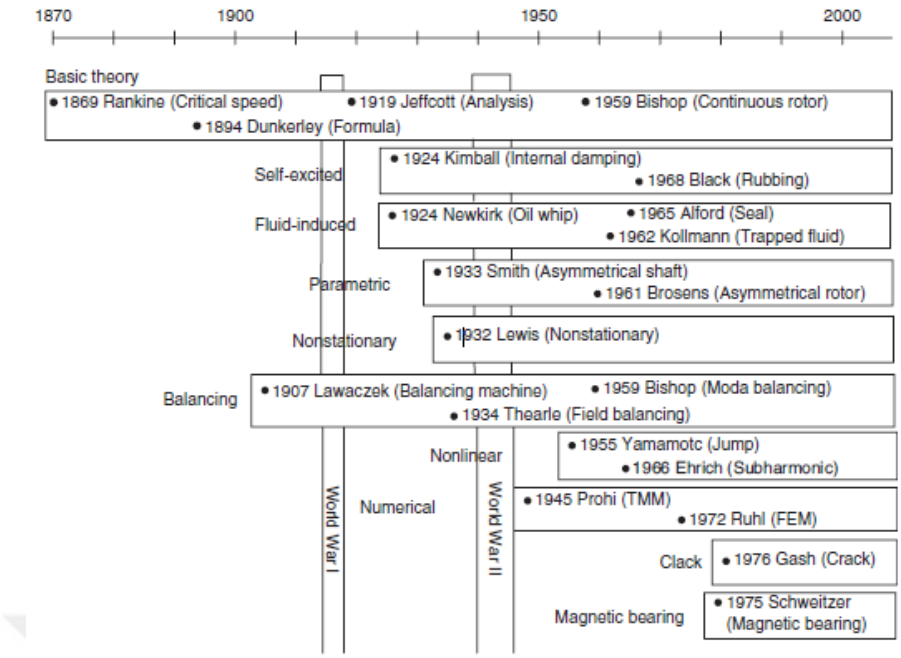

Figure 1.2: Historical development of rotordynamics [2].

At this point, Jeffcott Rotor worth explaining deeper as the definitions and derivations of this study are still keeps being referred to [3]. Some definitions can be found on Figure 1.3.

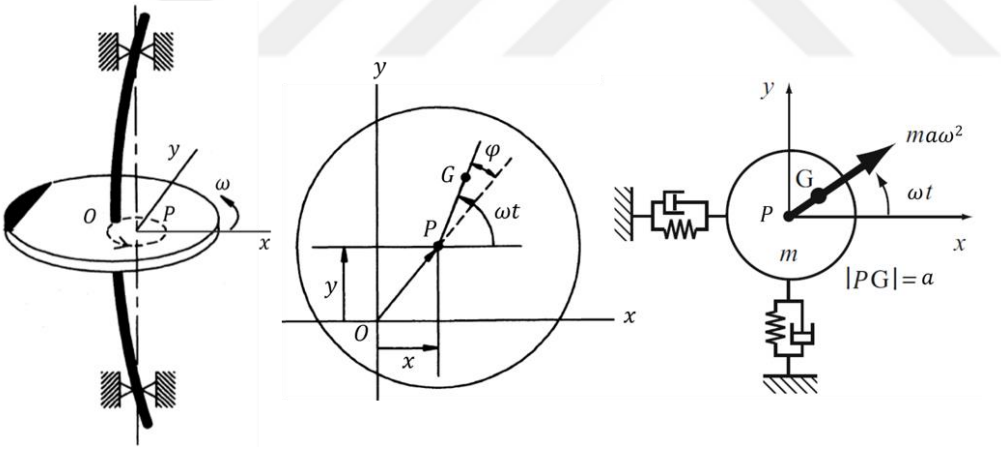

Figure 1.3: Jeffcott Rotor definitions [3]

For the above figure;

O: Bearing axis,

P: Centreline of the rotor,

G: Mass centre of the rotor,

a: Mass eccentricity.

Assuming a massless elastic shaft and equal spring and viscous damping coefficients on both directions, one can write the equation of motion as [4]:

$$m\ddot{x} + c\dot{x} + kx = ma\omega^2 \cos \omega t \tag{1.1}$$

$$m\ddot{y} + c\dot{y} + ky = ma\omega^2 \sin \omega t \tag{1.2}$$

Combine these two equations by introducing complex notation:

$$r = x + iy \tag{1.3}$$

So,

$$m\ddot{r} + c\dot{r} + kr = ma\omega^2 e^{i\omega t} \tag{1.4}$$

Now, one can obtain the characteristic equation by inserting $r = r_0 e^{\lambda t}$ into homogeneous differential equation,

$$(m\lambda^2 + c\lambda + k)r_0 = 0 \tag{1.5}$$

Solve for λ:

$$\lambda_{1,2} = -\zeta\omega_n \pm i\omega_n\sqrt{1-\zeta^2} \tag{1.6}$$

For $\zeta = 0$, $Im(\lambda_1) = \omega_n$ is called as forward natural frequency and $Im(\lambda_2) = -\omega_n$ is called as backward natural frequency.

It is possible to obtain unbalance response by inserting $r = r_u e^{i\omega t}$ into the equation of motion.

$$-m\omega^2 r_u + ic\omega r_u + kr_u = ma\omega^2 \tag{1.7}$$

Solve for r_u,

$$r_u = \frac{ma\omega^2}{(k - m\omega^2) + ic\omega} = \frac{a\frac{\omega^2}{{\omega_n}^2}}{\left(1 - \frac{\omega^2}{{\omega_n}^2}\right) + \left(2i\zeta\frac{\omega}{\omega_n}\right)} \tag{1.8}$$

And the orbit,

$$|r_u| = \frac{a\frac{\omega^2}{{\omega_n}^2}}{\sqrt{\left(1-\frac{\omega^2}{{\omega_n}^2}\right)^2+\left(2\zeta\frac{\omega}{\omega_n}\right)^2}} \tag{1.9}$$

Phase angle [3],

$$\varphi = \tan^{-1}\frac{Im(r_u)}{Re(r_u)} = \tan^{-1}\frac{c\omega}{k-m\omega^2} = \tan^{-1}\frac{2\zeta\frac{\omega}{\omega_n}}{1-\frac{\omega^2}{{\omega_n}^2}} \tag{1.10}$$

Critical speed: speed that makes synchronous unbalance response amplitude get its maximum value [4].

$$\frac{dr_u}{d\omega} = 0 \tag{1.11}$$

$$\omega_{cr} = \frac{2k}{\sqrt{4mk-2c^2}} = \frac{\omega_n}{\sqrt{1-2\zeta^2}} \tag{1.12}$$

To take the next step on explaining rotordynamics, a simple rotor supported by orthotropic bearings is a very useful model to visualize the so called forward and backward whirling motions. Let the studied model be the one at Figure 1.4.

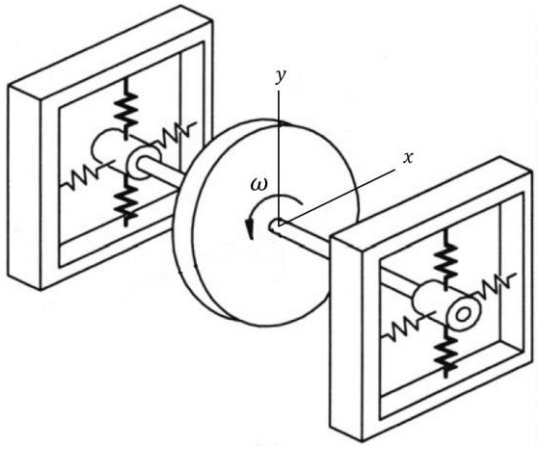

Figure 1.4: Simple rotor supported by orthotropic bearings [3].

Assuming a massless elastic shaft and equal spring and viscous damping coefficients on both directions, one can write the equation of motion as:

$$m\ddot{x} + k_x x = ma\omega^2 \cos \omega t \tag{1.13}$$

$$m\ddot{y} + k_y y = ma\omega^2 \sin \omega t \tag{1.14}$$

Here spring constants k_x and k_y are due to the stiffness of the shaft, bearing and supports. Simplify the equations of motion using complex notation:

$$m\ddot{r} + kr + \Delta k\bar{r} = ma\omega^2 e^{i\omega t} \tag{1.15}$$

Where;

$$r = x + iy \tag{1.16}$$

$$\bar{r} = x - iy \ \ (complex\ conjugate\ of\ r) \tag{1.17}$$

And;

$$k = \frac{k_x + k_y}{2} \tag{1.18}$$

$$\Delta k = \frac{k_x - k_y}{2} > 0 \tag{1.19}$$

Obtain characteristic equation by inserting $x = X_0 e^{\lambda t}$ and $y = Y_0 e^{\lambda t}$ into the homogenous differential equations.

$$m\lambda^2 + k_x = 0 \tag{1.20}$$

$$m\lambda^2 + k_y = 0 \tag{1.21}$$

So, the eigenvalues are:

$$\lambda_{1,2} = \mp i\omega_{nx} \tag{1.22}$$

$$\lambda_{3,4} = \mp i\omega_{ny} \tag{1.23}$$

Where;

$$\omega_{nx} = \sqrt{\frac{k_x}{m}} \tag{1.24}$$

$$\omega_{ny} = \sqrt{\frac{k_y}{m}} \tag{1.25}$$

Obtain unbalance response by inserting $r = r_f e^{i\omega t} + r_b e^{-i\omega t}$ into the equation of motion and solve for forward synchronous whirling radius r_f and backward synchronous whirling radius r_b [3].

$$r_f = \frac{a\omega^2(\omega_{nx}{}^2 + \omega_{ny}{}^2 - 2\omega^2)}{2(\omega_{nx}{}^2 - \omega^2)(\omega_{ny}{}^2 - \omega^2)} \tag{1.26}$$

$$r_b = \frac{a\omega^2(\omega_{nx}{}^2 - \omega_{ny}{}^2)}{2(\omega_{nx}{}^2 - \omega^2)(\omega_{ny}{}^2 - \omega^2)} \tag{1.27}$$

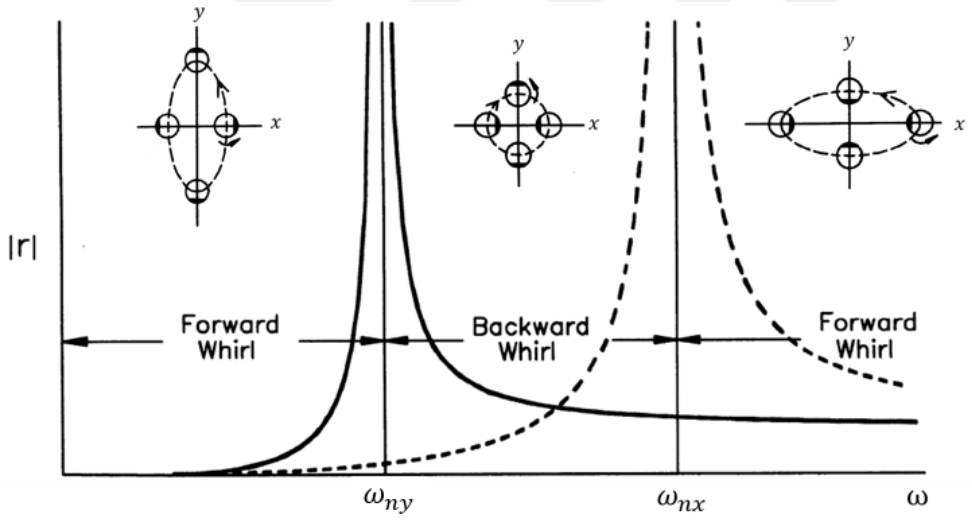

Figure 1.5: Forward and backward whirling motions [3].

As the name implies in the thesis' name, the study will consider the gyroscopic effect. To explain, consider a rigid body that has products of inertia equal to zero; there would only be the principal moments of inertia. Let the geometry be a disk, which means it is axisymmetric and its body diametral moments of inertia are equal to each other. Such a model can be seen in Figure 1.6.

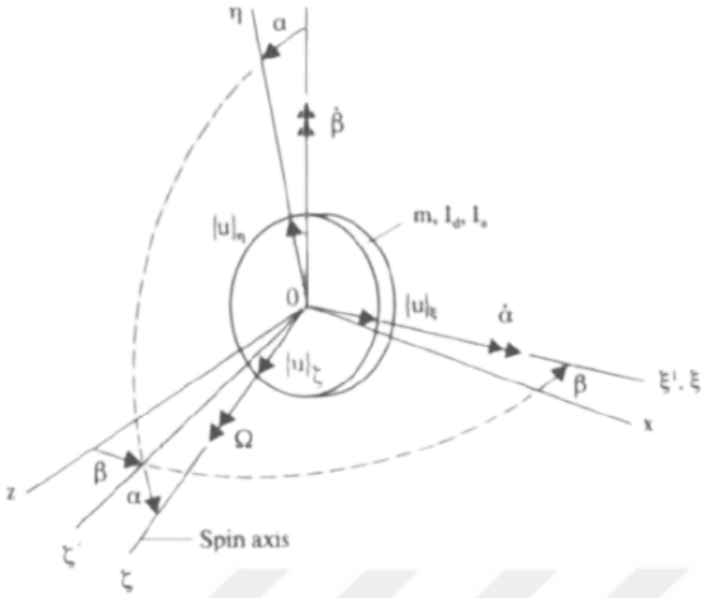

Figure 1.6: Definitions for a spinning disc [5].

If this disk is spinning around its z-axis with angular velocity ω, one can show using the Euler's equation that disk is subjected to the linearized moments in stationary coordinates as;

$$M_x = I_t\ddot{\theta}_x + I_p\omega\dot{\theta}_y + I_p\dot{\omega}\theta_y \tag{1.28}$$

$$M_y = I_t\ddot{\theta}_y - I_p\omega\dot{\theta}_x - I_p\dot{\omega}\theta_x \tag{1.29}$$

$$M_z = I_p\dot{\omega} \tag{1.30}$$

If $\dot{\omega} = 0$ [5]:

$$M_x = I_t\ddot{\theta}_x + I_p\omega\dot{\theta}_y \tag{1.31}$$

$$M_y = I_t\ddot{\theta}_y - I_p\omega\dot{\theta}_x \tag{1.32}$$

$$M_z = 0 \tag{1.33}$$

Now let there be a shaft with no mass eccentricity but the mass axis is displaced angularly where there is no eccentricity at the CoG, which can be seen on Figure 1.7.

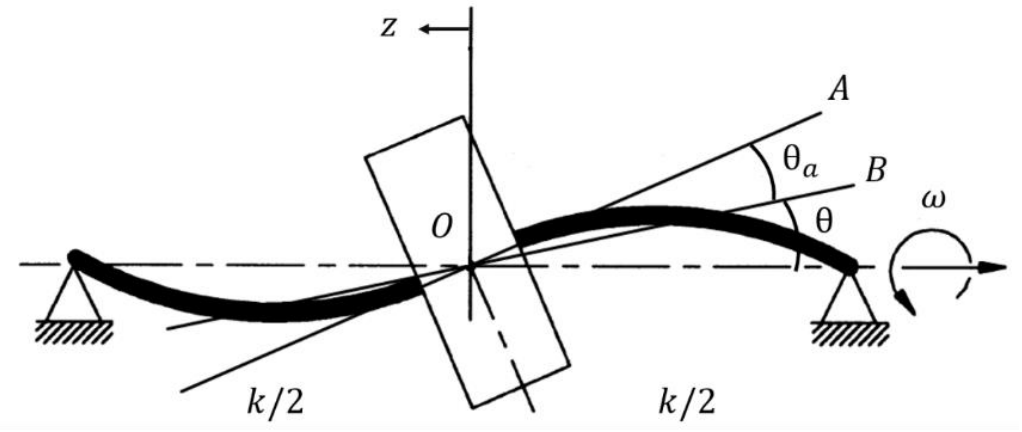

Figure 1.7: Shaft subjected to gyroscopic effect [4].

Here, OA is the disk centreline, OB is the tangential shaft direction and θ_a is the mass shift angle. Projections of θ on to xz and yz planes are θ_x and θ_y respectively. The rotor is supported by symmetrical torsional springs and dampers. For small θ_a angles, the equations of motion are as follows:

$$I_t\ddot{\theta}_x + I_p\omega\dot{\theta}_y + c_\theta\dot{\theta}_x + k_\theta\theta_x = (I_t - I_p)\theta_a\omega^2\cos\omega t \tag{1.34}$$

$$I_t\ddot{\theta}_y - I_p\omega\dot{\theta}_x + c_\theta\dot{\theta}_y + k_\theta\theta_y = (I_t - I_p)\theta_a\omega^2\sin\omega t \tag{1.35}$$

Introduce complex angle $\theta = \theta_x + i\theta_y$;

$$I_t\ddot{\theta} + c_\theta\dot{\theta} + k_\theta\theta - iI_p\omega\dot{\theta} += (I_t - I_p)\theta_a\omega^2 e^{i\omega t} \tag{1.36}$$

Let there be no damping and plug $\theta = \theta_0 e^{\lambda t}$ into the homogenous equation in order to get the characteristic equation;

$$I_t\lambda^2 - iI_p\omega\lambda + k_\theta = 0 \tag{1.37}$$

Eigenvalues can be found as [4]:

$$\lambda_{1,2} = \frac{i\left(I_p\omega \mp \sqrt{{I_p}^2\omega^2 + 4I_t k_\theta}\right)}{2I_t} \tag{1.38}$$

As can be seen, eigenvalues; thus, natural frequencies of rotor system with gyroscopic effect are functions of rotational speed.

The mentioned topics are enough to cover the basics of rotordynamics which are related to balancing directly. Modeling of rotor systems can be extended much further, but these are not subjects for this study.

Further modeling approaches may include modeling damping at both bearings as well as supporting structure by also considering anisotropic stiffness, damping or cross terms. These should introduce stability definitions for the systems as well as an isotropic behavior definition, which is a function of rotational speed. Modeling at cylindrical coordinates considering asymmetrical stiffness, as well as considering gravitational force, could again introduce unstable operating ranges and subharmonic resonance definition. Internal and external damping modeling will, again, introduce unstable zones for the rotating hardware. Rotors with asymmetrical inertia, which find applications in electric motors, for example, are also another interesting topic and have, again, unstable zones [3].

The next topic to investigate is balancing. Jeffcott was the first researcher to point out the importance of balancing in his paper in 1919, which was mentioned in the earlier sections. No contribution was made until the 1930s for balancing. Until the 1950s, research about balancing involved techniques of rigid balancing [4]. The necessity of flexible balancing had risen with the development of the first jet engines. Many projects went on around the 1930s and 1940s, but the first fully operational aircraft with a jet engine was the Germans' Messerschmitt Me 262, which entered the service at the latest stages of WW2. The 1940s also saw a rise in the usage of steam turbines as well. These technologies became widespread throughout the 1940s and common vibration problems led the researchers to dive deep into balancing.

As explained before, a rigid rotor operates significantly less than its first critical bending speed and a flexible rotor operates close to or above its first critical bending speed.

On of the first examples of rigid rotor balancing discussion can be found at Timoshenko's paper at 1928. He described some rigid rotor balancing machines of his era. He pointed out the necessity of unique balancing techniques for flexible balancing but could not introduce a solution.

Another researcher who studied the rigid balancing of early stages is Den Hartog. He released a paper in 1934 that focused on rigid balancing techniques as well as balancing machines.

In the early stages of the 1940s, two research papers were released by Kroon, which targeted to be a design guide for rotating components. These papers were important since Kroon explained the synchronous rotor excitation and the necessity of both rigid and flexible balancing in his first publication. In his second paper, he explained some balancing techniques and machines. He also proposed the usage of a graphic method for flexible balancing [4].

Flexible balancing is used to balance so-called flexible rotors. The types of flexible balancing can be divided into two general sections, namely "modal balancing" and "influence coefficient balancing." Modal balancing was developed earlier than influence coefficient balancing. Practices for both approaches have changed over the years and still different types, which can still considered to be inside these two sections, are being used.

In 1953, Grobel proposed a method for flexible balancing of turbine-generator rotors. This method was an earlier version of modal balancing and it required the usage of trial masses. In 1954, Meldal introduced the orthogonality conditions for rotor response and set the basis for modal balancing.

Bishop is the researcher to use the term modal balancing for the first time. He published a series of research with some other researchers starting from 1957 to 1970s. His first papers described both the theory and practical application of modal balancing. He used Jeffcott's rotor to derive a modal expansion of the synchronous vibrations of a lightly damped rotor. He, with the help of some other researchers, kept publishing papers targeting the practical issues faced in balancing. He explained cases including axisymmetric rotors, shafts with non-uniform cross-sections, shafts with a bow, not isolated modes, effect of gravity, and anisotropic bearings. All his works required the usage of trial masses.

Gasch and Drechser introduced a modified modal balancing method that required no trial mass. He used the analytically generated modal properties combined with test data collected at a number of critical speeds. Saito and Azawa introduced a method of

modal balancing where complex modes are used in the presence of viscous damping [2] [4].

In 1934, Thearle introduced a field balancing method that could be accepted as a basis for the influence coefficients method. Although he was not targeting to balance flexible rotors, his approach was successful at balancing some simple flexible rotors.

The first generalized influence coefficients method was developed by Goodman in 1964 in the USA. His method was developed mainly thanks to the progress of computers. He used least-squares and weighted least-squares solutions to obtain influence coefficients. Little and Pilkey introduced a modified approach by using the linear programming approaches. Larsson, in 1976, advised a statistical solution for calculating influence coefficients using multiple sets of trial masses with the usage of a linear regression analysis [2] [4].

Parkinson, Darlow, Smalley and Badgley released some research defining a combined approach between modal balancing and influence coefficient balancing called the "Unified Balancing Approach". This method used modal properties, which are obtained using test data to enhance and modify influence coefficient balancing [4].

1.2 Purpose of Thesis

This study will be targeted to obtain a new flexible balancing approach that is both robust and precise. In order to achieve that, studies of previous researchers in areas such as rotordynamics, FEM, balancing and numerical methods need to be understood well. This approach will be based on a mix of analytical and numerical approaches. In summary, the balancing procedure developed consists of steps such as;

Obtaining the 1D FE model of the rotor system.

Running the unbalanced rotor assembly close to the first critical speed and measuring displacement data.

Feeding FE model and displacement history to a modified Augmented Kalman Filter algorithm.

Obtaining induced unbalance forces at desired balancing planes.

Adding or removing the first unbalance masses.

Repeating the process for each mode and acquiring the necessary balancing masses with the help of a modal approach.

The whole process covers the application of the gyroscopic effect.

2. THEORY

This chapter will provide the theoretical background of the solution proposed for flexible balancing. Various research and theoretical fundamentals will be brought at areas such as; vibrations, rotordynamics, the strength of materials and signal processing.

2.1 Unbalance Force

In order to make the flexible balancing, it is assumed that the rotating machinery has excitations only due to mass unbalance. Thus, it is a good starting point to define the form of unbalance force so that it is well understood the main purpose of the work being done in this study. Consider the slice of a rotor, which can be seen below in Figure 2.1. Unbalance force should cause lateral vibrations and whirling movement. For this reason, it must be studied in two dimensions, which are the lateral directions.

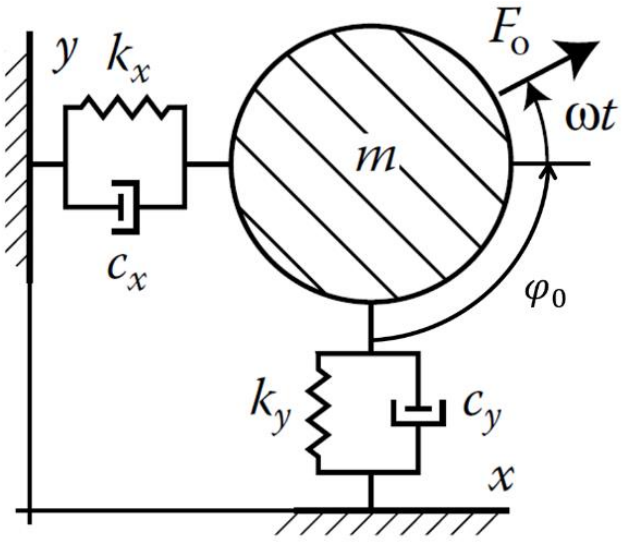

Figure 2.1: Slice of a rotor [6].

Assume the magnitude of unbalance force is time-invariant, i.e., does not change with time. In reality; the magnitude of unbalance force might change in certain systems, such as magnetic force at electric motors, dust contamination at fans or unsymmetrical

rotors. So, for our case, which is a general situation for balancing problems, it is enough to assume a time-invariant magnitude of mass unbalance force. Since the mass unbalance is at a certain location on the rotor, i.e., it has a certain distance of eccentricity from the rotational axis, the force will rotate as the rotor rotates. This means that the vector of unbalance force is dependent on rotational speed and the angular position of the rotor; thus, it is time-dependent. If F_0 is the unbalance force and φ_0 is the angular position of the mass unbalance, excitation force at two directions can be shown as [6]:

$$f_x = F_0 \cos(\omega t + \varphi_0) \tag{2.1}$$

$$f_y = F_0 \sin(\omega t + \varphi_0) \tag{2.2}$$

The magnitude of the unbalance force can be described using the definitions of centrifugal force:

$$F_0 = U\omega^2 \tag{2.3}$$

Here, U is the unbalance and can be described as:

$$U = ma \tag{2.4}$$

Thus;

$$F_0 = ma\omega^2 \tag{2.5}$$

Is the magnitude of the unbalance force. So, the unbalance force is:

$$f_x = ma\omega^2 \cos(\omega t + \varphi_0) \tag{2.6}$$

$$f_y = ma\omega^2 \sin(\omega t + \varphi_0) \tag{2.7}$$

Here, m is the unbalance mass and a is the eccentricity in units of distance. It should be pointed out that any kind of balancing operation would target to identify unbalance U and phase angle φ_0. It is also important to mention that what is described above is a slice of the rotating hardware. Thus, the real case has a continuous unbalance force distribution over the axial direction of the shaft.

2.2 Rotordynamics Equation of Motion

Consider a rotating shaft with an eccentricity profile $a(z)$, which can be seen in Figure 2.2. The shaft has an elasticity modulus of E, cross section of A, density of ρ, length of l and second moment of inertia of I_t. There are bearings at known axial locations with generalized stiffness and damping terms. There are balance masses added at k different locations.

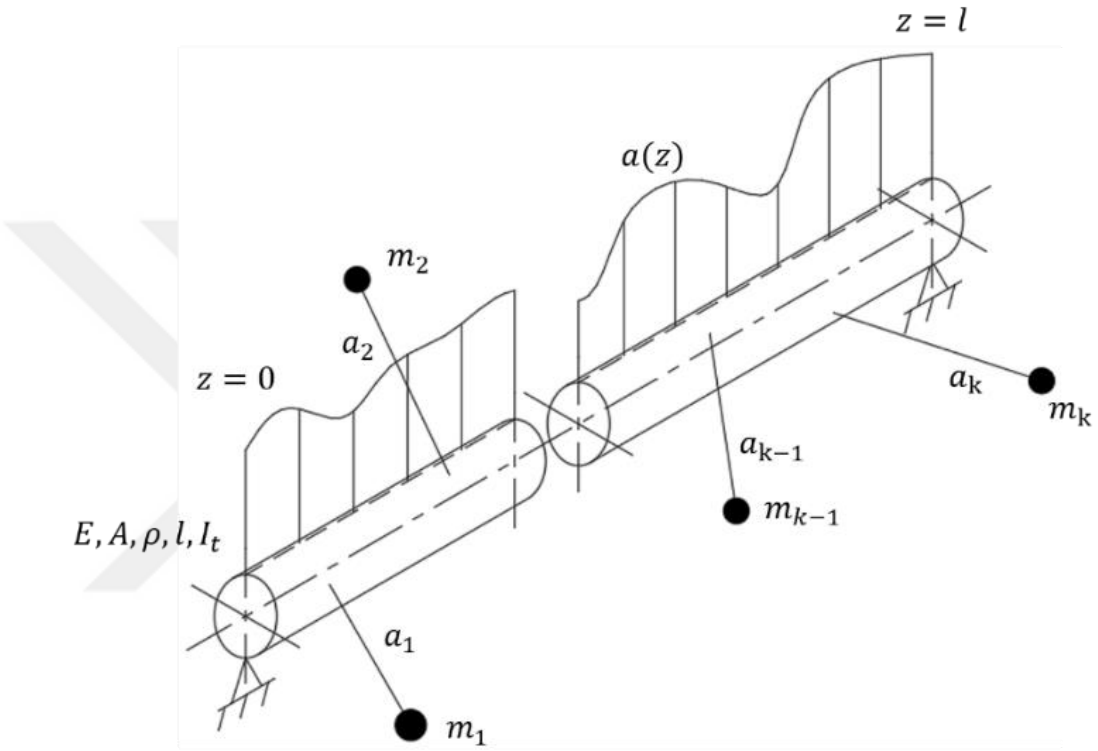

Figure 2.2: Representation of a rotating shaft with unbalance.

Let any kind of term described above be in general form such that terms could be functions of time or axial position. For such a system, an equation of motion could be in the form [7]:

$$[M]\{\ddot{x}\} + ([C] + [G])\{\dot{x}\} + [K]\{x\} = \{f(t)\} \tag{2.8}$$

For the above equation:

$\{x\}$: vector of displacements and rotations,

$[M]$: mass matrix,

$[C]$: damping matrix,

$[G]$: gyroscopic matrix,

$[K]$: stiffness matrix,

$\{f(t)\}$: vector of excitation forces and moments.

Notice the equation of motion given is in discrete form. It is also possible to model this system in continuous form as well. Since the area of interest of this study is balancing, it is found more appropriate to use discrete modeling. This is highly due to rotating systems having a complex structure, e.g., with lots of steps on shafts, mounted multiple discs and multiple bearing locations. Considering the known and unknown values and order of the governing differential equations, continuous modeling introduces a huge amount of computational cost and also requires a lot of modeling effort. Instead, the study will be made using the FEM, which has a theory that is very well-known and adequate to model any kind of structure for both time-dependent and time-invariant properties. It is also suitable for usage with the Kalman Filter, which is the most sophisticated part of the balancing method introduced here.

More details on high-level continuous rotor modeling can be found in references [8] and [9].

For the discrete approach, terms can be easily arranged so that a change of properties on axial direction is considered. The balancing method proposed will use only gyroscopic terms and excitation terms as time-dependent. This introduces a nonlinear nature to the problem since gyroscopic terms are functions of rotational speed; thus, the function of time and unbalance force changes its direction by time. Damping will be ignored since it is very complicated to model accurately. So, the final equation of motion seems as follows:

$$[M]\{\ddot{x}\} + [G(\omega)]\{\dot{x}\} + [K]\{x\} = \{f(t)\} \tag{2.9}$$

A modal approach to such a system can still be somehow possible in fixed-speed cases. The reason for using fixed speed cases is that the modal analysis can only be done for linear systems, but the above system has nonlinearity. When the rotational speed is fixed, the gyroscopic matrix is also fixed so that it can be considered to be linear at this point. Under these circumstances, the phrase “complex eigenvalue analysis” is

used instead of modal analysis since the system has also terms multiplied by $\{\dot{x}\}$. Complex eigenvalue can be done for [10]:

$$[M]\{\ddot{x}\} + [G(\omega)]\{\dot{x}\} + [K]\{x\} = 0 \tag{2.10}$$

Let;

$$\{x\} = \{X\}e^{\lambda t} \tag{2.11}$$

And plug this into (2.10) for a fixed-speed case:

$$([M]\lambda^2 + [G(\omega)]\lambda + [K])\{X\} = 0 \tag{2.12}$$

In order to get mass-normalized mode shapes:

$$(\lambda^2 + [M]^{-1}[G(\omega)]\lambda + [M]^{-1}[K])\{X\} = 0 \tag{2.13}$$

But preferably, an eigenvalue problem should be in the form of:

$$([A] - \lambda[I])\{\bar{X}\} = 0 \tag{2.14}$$

To obtain such a form it is suggested that [10]:

$$[A] = \begin{bmatrix} 0 & I \\ [M]^{-1}[K] & [M]^{-1}[G(\omega)] \end{bmatrix} \tag{2.15}$$

$$\{\bar{X}\} = \begin{Bmatrix} \{X\} \\ \lambda\{X\} \end{Bmatrix} \tag{2.16}$$

Which is twice the size the system DoF. Now it can be said that:

$$det([A] - \lambda[I]) = 0 \tag{2.17}$$

Eigenvalues and eigenvectors can be found then using the regular approach. One thing to note is that an eigenvalue and an eigenvector will be found in a duplicate manner when using complex eigenvalue analysis. Thus, some portion of post-processing is necessary. Eigenvalues will be in complex notation, which would mean a phase difference when calculating the system response. More detail will not be given in this

study since the theory of complex eigenvalue analysis is very well-known and can be found in many sources.

For the balancing approach introduced in this study, both the direct approach and the modal approach will be used in different steps. Kalman Filter will be run using a direct approach and balancing conditions will be set using modal properties at critical speeds.

2.3 Creating A Finite Element Model

As mentioned earlier, the balancing approach introduced here is going to have an implementation of FEM and it is highly due to having a lower computational cost. Now, then, let us make the necessary definitions for a rotordynamics FE model. It was shared that only the unbalance forces will be taken into account for the study. This means it is adequate to have a FE model which considers only lateral movements. So, the necessary formulation is the beam formulation. A rotordynamics beam element with the notation that is being followed in this study can be seen in Figure 2.3.

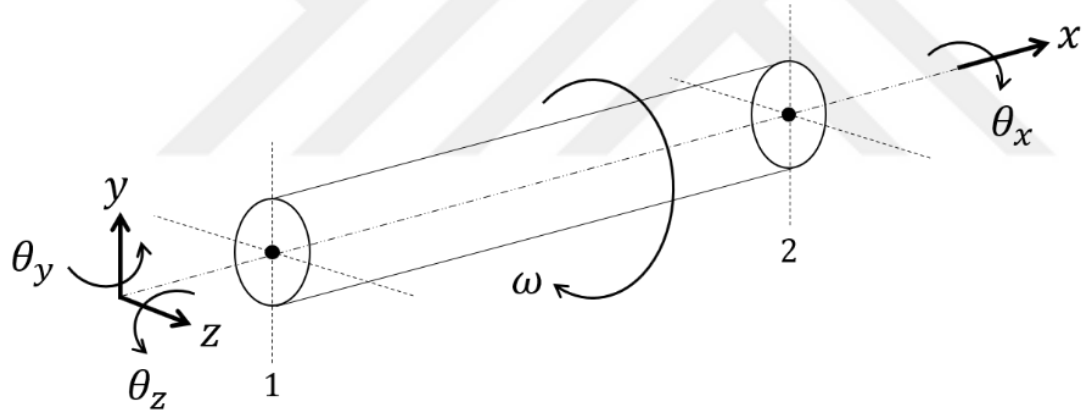

Figure 2.3: Rotordynamics beam element.

One can understand from Figure 2.3 that each beam node has 4 DoF and a beam element has 8 DoF. Then, the displacement vector is at the following structure:

$$\{x\} = \left[y_1\ z_1\ \theta_{y1}\ \theta_{z1}\ y_2\ z_2\ \theta_{y2}\ \theta_{z2}\right]^T \tag{2.18}$$

The simplest beam element formulation is the Euler-Bernoulli Beam Formulation. According to the Euler-Bernoulli Beam Theory, elemental matrixes are as [11]:

$$[M] = \begin{bmatrix} \frac{13}{35} & 0 & 0 & \frac{11\ell}{210} & \frac{9}{70} & 0 & 0 & \frac{-13\ell}{420} \\ 0 & \frac{13}{35} & \frac{-11\ell}{210} & 0 & 0 & \frac{9}{70} & \frac{13\ell}{420} & 0 \\ 0 & \frac{-11\ell}{210} & \frac{\ell^2}{105} & 0 & 0 & \frac{-13\ell}{420} & \frac{-\ell^2}{140} & 0 \\ \frac{11\ell}{210} & 0 & 0 & \frac{\ell^2}{105} & \frac{13\ell}{420} & 0 & 0 & \frac{-\ell^2}{140} \\ \frac{9}{70} & 0 & 0 & \frac{13\ell}{420} & \frac{13}{35} & 0 & 0 & \frac{-11\ell}{210} \\ 0 & \frac{9}{70} & \frac{-13\ell}{420} & 0 & 0 & \frac{13}{35} & \frac{11\ell}{210} & 0 \\ 0 & \frac{13\ell}{420} & \frac{-\ell^2}{140} & 0 & 0 & \frac{11\ell}{210} & \frac{\ell^2}{105} & 0 \\ \frac{-13\ell}{420} & 0 & 0 & \frac{-\ell^2}{140} & \frac{-11\ell}{210} & 0 & 0 & \frac{\ell^2}{105} \end{bmatrix} \rho A\ell \qquad (2.19)$$

$$[K] = \begin{bmatrix} 12 & 0 & 0 & 6\ell & -12 & 0 & 0 & 6\ell \\ 0 & 12 & -6\ell & 0 & 0 & -12 & -6\ell & 0 \\ 0 & -6\ell & 4\ell^2 & 0 & 0 & 6\ell & 2\ell^2 & 0 \\ 6\ell & 0 & 0 & 4\ell^2 & -6\ell & 0 & 0 & 2\ell^2 \\ -12 & 0 & 0 & -6\ell & 12 & 0 & 0 & -6\ell \\ 0 & -12 & 6\ell & 0 & 0 & 12 & 6\ell & 0 \\ 0 & -6\ell & 2\ell^2 & 0 & 0 & 6\ell & 4\ell^2 & 0 \\ 6\ell & 0 & 0 & 2\ell^2 & -6\ell & 0 & 0 & 4\ell^2 \end{bmatrix} \frac{EI}{\ell^3} \qquad (2.20)$$

$$[G(\omega)] = \begin{bmatrix} 0 & -36 & 3\ell & 0 & 0 & 36 & 3\ell & 0 \\ 36 & 0 & 0 & 3\ell & -36 & 0 & 0 & 3\ell \\ -3\ell & 0 & 0 & -4\ell^2 & 3\ell & 0 & 0 & \ell^2 \\ 0 & -3\ell & 4\ell^2 & 0 & 0 & 3\ell & -\ell^2 & 0 \\ 0 & 36 & -3\ell & 0 & 0 & -36 & -3\ell & 0 \\ -36 & 0 & 0 & -3\ell & 36 & 0 & 0 & -3\ell \\ -3\ell & 0 & 0 & \ell^2 & 3\ell & 0 & 0 & -4\ell^2 \\ 0 & -3\ell & -\ell^2 & 0 & 0 & 3\ell & 4\ell^2 & 0 \end{bmatrix} \frac{\rho I\omega}{15\ell} \qquad (2.21)$$

Euler-Bernoulli beams are found to be giving accurate results with slander shafts, i.e., shafts with lower cross-section to length ratio. As the slenderness decreases, Euler-Bernoulli beams can not capture the effect of shear deformation. For that reason, the Timoshenko Beam Theory is more appropriate to use with shafts that have lower slenderness. Timoshenko Beam Theory is again a very well-known theory and formulations can be found on many sources.

Note that for the above formulations, mass and stiffness matrixes are symmetrical matrixes, but the gyroscopic matrix is a skew-symmetric matrix.

A rotor model must also include the effect of bearings, foundations and mounted rotating discs. For this application, it is found adequate to ignore the inertial effects of bearings and foundations as well as the stiffness effects of rotating discs. Thus, one has to make sure that also bearing stiffness, foundation stiffness and disc inertias are also included in the model. This can be ensured with the small modifications at the global matrixes. These effects will be modeled in a manner such as in Figure 2.4.

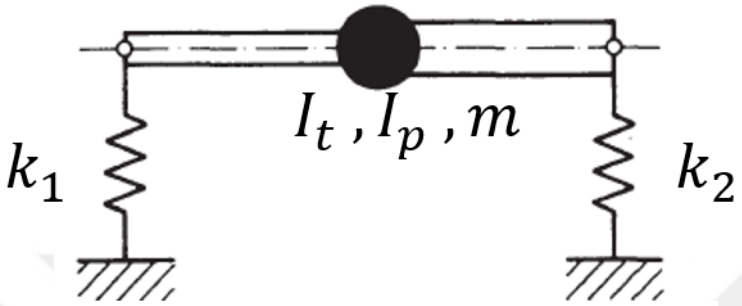

Figure 2.4: Modelling approach for 1D elements with FEM [7].

For massless spring elements, additional properties must be input to a node such as [7] [11]:

$$[K] = \begin{bmatrix} k_{1,y} & 0 & 0 & 0 \\ 0 & k_{1,z} & 0 & 0 \\ 0 & 0 & 0 & 0 \\ 0 & 0 & 0 & 0 \end{bmatrix} \tag{2.22}$$

Other types of springs can also be modeled in the same manner, as well as foundation stiffnesses. For rigid discs, 1D element formulation is as follows:

$$[M] = \begin{bmatrix} m & 0 & 0 & 0 \\ 0 & m & 0 & 0 \\ 0 & 0 & I_t & 0 \\ 0 & 0 & 0 & I_t \end{bmatrix} \tag{2.23}$$

$$[G(\omega)] = \begin{bmatrix} 0 & 0 & 0 & 0 \\ 0 & 0 & 0 & 0 \\ 0 & 0 & 0 & -I_p \\ 0 & 0 & I_p & 0 \end{bmatrix} \omega \tag{2.24}$$

When the element properties are known, the only step left is to form the global matrixes. For a rotordynamics beam element formulation, this is done by setting element lengths and determining corresponding properties for each element. After the

system is discretized, global matrixes are formed by adding each elemental matrix next to one another and by stacking properties if there are elements that are communicating with each other. This process can be visualized as in Figure 2.5.

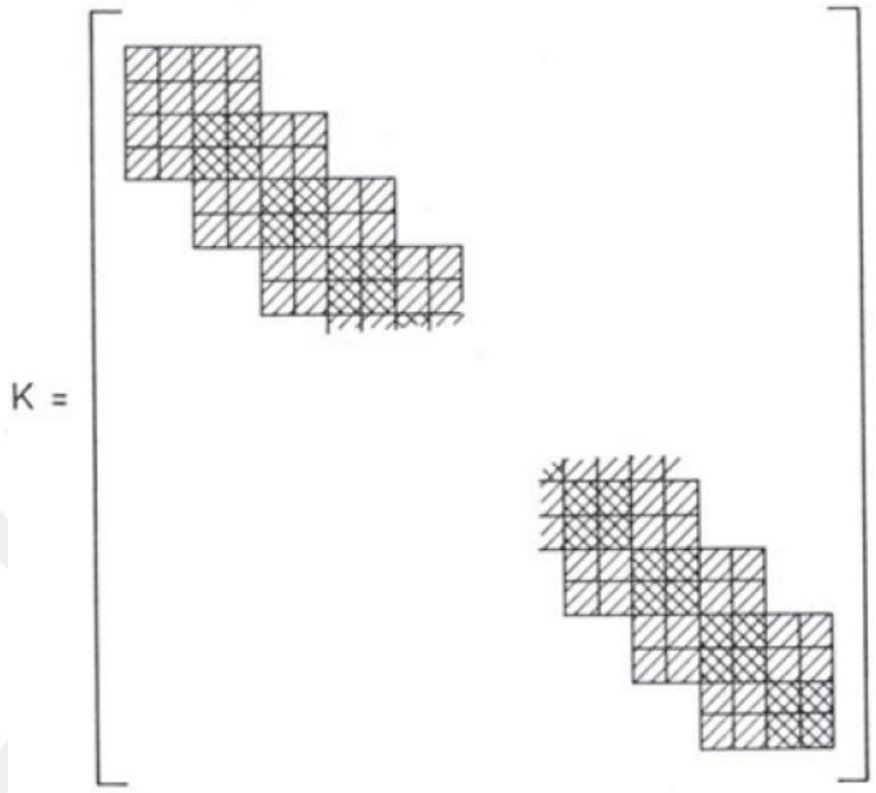

Figure 2.5: Stacking elemental matrixes to form global matrix [7].

2.4 Dynamic Force Estimation

Estimation of structural forces has happened to be a challenge and very dependent on application. There are various factors that decide to performance of dynamic force estimation approaches. Examples can be given as; area of application, quality of measured data or type of dynamic force. The balancing method suggested in this study requires the usage of a robust force identification technique to generate the unbalance forces. Thus, research in the area has been made. In summary, there are a few different approaches to the problem. These include approaches at time domain, frequency domain or statistical approaches [12]. Some examples can be given below.

The first method to be explained is “Matrix Inversion”. Consider a mechanical system in that outputs are measured at *m* different locations and these are excited at *n* different locations. For a linear vibratory system, the following equation can be written [12]:

$$X(\omega) = H(\omega)F(\omega) \tag{2.25}$$

Here; *X* is the measured response in the frequency domain, *H* is the FRF of this system and *F* is the load vector to be identified. From the modal analysis theory:

$$H_{ij}(\omega) = \sum_{k=1}^{N} \frac{\phi_{ik}\phi_{jk}}{m_k({\omega_k}^2 - \omega^2 + 2j\zeta_k\omega_k\omega)} \tag{2.26}$$

Considering the above equations; if the FRF of the system is known or could be generated and if *X* could be measured, it can be said that it is possible to obtain structural forces.

The next method is the "Sum of Weighted Accelerations" approach. This approach tries to identify the excitation forces by summing measured accelerations, which are multiplied with a weight coefficient such that [13]:

$$F(t) = \sum_{i=1}^{n} W_i A_i(t) \tag{2.27}$$

Here, *W* is the weight coefficient and *A* is the measured acceleration data. By applying a known excitation force to the system, it can be possible to determine the weight coefficients. Since *A* is being measured:

$$[W] = ([A]^T[A])^{-1}[A]^T[F] \tag{2.28}$$

With a discretized form:

$$[F] = [B][W] \tag{2.29}$$

Where *B* is the new acceleration response.

This approach can be implemented in both linear and nonlinear systems. One of the main advantages of the approach happens to be it does not require any knowledge of the system properties.

Now, to come to the "Pseudo Inverse Method", consider a vibratory system such that [13]:

$$[M]\{\ddot{x}\} + [C]\{\dot{x}\} + [K]\{x\} = \{f(t)\} \tag{2.30}$$

It can be said that;

$$\{\ddot{x}(\omega)\} = [H(\omega)]\{F(\omega)\} \tag{2.31}$$

$$[H(\omega)] = \frac{\ddot{x}(\omega)F^*(\omega)}{F(\omega)F^*(\omega)} = \frac{Cross\ Spectrum}{Auto\ Spectrum} \tag{2.32}$$

Here; $\ddot{x}(\omega)$ is the response acceleration at the frequency domain, *F* is the input force spectrum and "*" donates the complex conjugate of a matrix. In order to make this method work, the FRF of the system must be obtained by the usage of known forces. Once the FRF is known, any unknown input can be obtained using:

$$\{F(\omega)\} = pinv([H(\omega)])\{\ddot{x}(\omega)\} \tag{2.33}$$

$$pinv([H(\omega)]) = ([H(\omega)]^*[H(\omega)])^{-1}[H(\omega)]^* \tag{2.34}$$

The final approach is the "Kalman Filter". This method is a recursive linear state estimator which tries to optimize the values in a minimum covariance-based manner by also taking into account system uncertainty. In principle, a value named "Kalman Gain" is used to converge the values by modifying them at each time step. Consider a system that is in the state-space form such that [12] [13]:

$$X(t) = AX(t) + BF(t) \tag{2.35}$$

$$Y(t) = CX(t) + DF(t) \tag{2.36}$$

Here; *A* is the system matrix, *B* is the input matrix, *C* is the output matrix, *D* is the feedthrough matrix (which is equal to zero for structural dynamics), *X* is the state vector, *Y* is the observation vector and *F* is the forcing vector. Kalman Filter procedure can be shown as follows, starting with the prediction phase:

$$X_k^- = AX_{k-1}^+ + BF_{k-1} \tag{2.37}$$

$$P_k^- = AP_{k-1}^+A^T + Q \tag{2.38}$$

Now the update phase:

$$Z_k = Y_k - CX_k^- \tag{2.39}$$

$$K_k = P_k^- C^T (R + CP_k^- C^T)^{-1} \tag{2.40}$$

$$X_k^+ = X_k^- + K_k Z_k \tag{2.41}$$

$$P_k^+ = (I - K_k C) P_k^- \tag{2.42}$$

At these equations, "-" means estimation and "+" means updated estimation. Here; *P* is the error covariance, *Q* is the process noise covariance, *R* is the measurement noise covariance, *Z* is the measurement residual and *K* is the Kalman Gain.

This method is suitable for linear systems, but Kalman Filter has further studies, such as Augmented Kalman Filter and Extended Kalman Filter, which are suitable for nonlinear applications or some other applications as well. It is decided to use the Kalman Filter for this study; the competitive advantage of this method is it is a recursive linear state estimator that tries to optimize the values in a minimum covariance-based manner by also taking into account system uncertainty. For the balancing method studied here, the Kalman Filter is the most sophisticated addition to what is being used currently. The main reason for the usage of the Kalman Filter is its ability to estimate the unknown states of the system. This is done by feeding FE matrixes inside the Kalman Filter as well as providing measurement data from a rotor test rig or a rotor on-site. Thanks to this ability, the Kalman Filter will be fed with displacement data from the limited amount of DoFs, which will be enough to accurately estimate the state of other unknown DoFs.

2.4.1 Space state representation

So far, an equation of motion that is in the form:

$$[M]\{\ddot{x}\} + [G(\omega)]\{\dot{x}\} + [K]\{x\} = \{f(t)\} \tag{2.43}$$

Is developed. But this equation of motion is not in state space representation. Space state representation should be in the form [14]:

$$\{x\} = [A]\{x\} + [B]\{f\} \tag{2.44}$$

$$\{y\} = [C]\{x\} + [D]\{f\} \tag{2.45}$$

Where:

$$\{x\} = [\{x\}\ \{\dot{x}\}]^T \tag{2.46}$$

$$[A] = \begin{bmatrix} 0 & I \\ -[M]^{-1}[K] & -[M]^{-1}[G(\omega)] \end{bmatrix} \tag{2.47}$$

$$[B] = \begin{bmatrix} 0 \\ -[M]^{-1} \end{bmatrix} \tag{2.48}$$

$$[C] = [I \quad 0] \tag{2.49}$$

$$[D] = [0] \tag{2.50}$$

These matrixes are named as:

$[A]$: System matrix,

$[B]$: Input matrix,

$[C]$: Output (measurement) matrix,

$[D]$: Feedthrough matrix.

These definitions are made according to the application area. Since the measurement data is said to be displacement, the measurement matrix has an identity matrix on the left-hand side. If it happened to be velocity data, then the identity matrix would be on the right-hand side. It is also possible to feed these two into the system together. Also, the feedthrough matrix is a zero matrix since this is an application of structural dynamics.

One important point to mention here is that, these matrixes are not in discretized form at the time being for the state space representation. A further arrangement must be made in order to make sure that the matrixes are in the discretized form. A discretized space state representation would be in the form:

$$\{x\}_k = [A_d]\{x\}_{k-1} + [B_d]\{f\}_{k-1} \tag{2.51}$$

$$\{y\}_k = [C_d]\{x\}_k \tag{2.52}$$

Where k is the current time step and [15]:

$$[A_d] = e^{[A]t} \tag{2.53}$$

$$[B_d] = ([A_d] - [I])[A]^{-1}[B] = \left(\int_0^{\Delta t} e^{[A]t}dt\right)[B] \tag{2.54}$$

$$[C_d] = [C] \tag{2.55}$$

Here, using Taylor Series Expansion:

$$e^{[A]t} = [I] + [A]\Delta t + \frac{([A]\Delta t)^2}{2!} + \frac{([A]\Delta t)^3}{3!} + \frac{([A]\Delta t)^4}{4!} + \cdots \tag{2.56}$$

And by using Power Series:

$$\int_0^{\Delta t} e^{[A]t}dt = \Delta t\left([I] + \frac{[A]\Delta t}{2!} + \frac{([A]\Delta t)^2}{3!} + \frac{([A]\Delta t)^3}{4!} + \cdots\right) \tag{2.57}$$

After applying these, matrix definitions for Kalman Filter will be discretized and will be ready to use as inputs.

2.4.2 Kalman Filter application

Now that the discretized matrixes are obtained, the Kalman Filter algorithm can be written in a discrete format. Note that k is the current time step, n is the total number of DoFs the system has and m is the total DoFs that are being measured.

Prediction phase [16]:

$$\{x\}_k^- = [A_d]\{x\}_{k-1}^+ + [A_d]\{f\}_{k-1} \tag{2.58}$$

$$[P]_k^- = [A_d][P]_{k-1}^+[A_d]^T + [Q] \tag{2.59}$$

Update phase:

$$\{z\}_k = \{y\}_k - [C_d]\{x\}_k^- \tag{2.60}$$

$$[K_k] = [P]_k^-[C_d]^T([R] + [C_d][P]_k^-[C_d]^T)^{-1} \tag{2.61}$$

$$\{x\}_k^+ = \{x\}_k^- + [K]_k[z]_k \tag{2.62}$$

$$[P]_k^+ = ([I] - [K]_k[C_d])[P]_k^- \tag{2.63}$$

Dimensions of these matrixes are as follows:

$\{x\}$: 2n x 1,

$\{f\}$: n x 1,

$\{y\}$: m x 1,

$[A_d]$: 2n x 2n,

$[B_d]$: 2n x n,

$[C_d]$: m x 2n,

$[P]$: 2n x 2n,

$[Q]$: 2n x 2n,

$[R]$: m x m,

$[K]$: 2n x m,

$\{z\}$: m x 1.

It was mentioned earlier that the general rotordynamics equation is in nonlinear form due to the consideration of a gyroscopic effect. Another mention should be made that the current state estimation is targeting displacement and velocity values. It must be understood that what is being tried to do here is to obtain unbalance forces. Up to this point, it is possible to obtain unknown displacement and velocities, but in order to obtain unbalance forces, additional applications are necessary. In general, these are called as force reconstruction methods. There are different methods, as explained in the earlier sections. One application that is found to be very useful at this point is, rather than an additional method, a trick in Kalman Filter formulation. This trick is changing this formulation into an Augmented Kalman Filter formulation.

2.4.3 Augmented Kalman Filter

The benefit of the Augmented Kalman Filter comes into play when it is wanted to estimate forces. This technique is actually no different than a standard Kalman Filter, but the state vector is replaced by and expanded vector, which also consists of forces and moments. The rest of the formulation and matrixes are rearranged accordingly.

Consider a new state vector such that [17]:

$$\{x^*\} = [\{x\}\ \{\dot{x}\}\ \{f\}]^T \tag{2.64}$$

The new discrete state space representation will be in the form:

$$\{x^*\}_k = [{A_d}^*]\{x^*\}_{k-1} \tag{2.65}$$

$$\{y\}_k = [{C_d}^*]\{x^*\}_k \tag{2.66}$$

Note that there are no force terms as it is defined inside the state vector. Here;

$$[{A_d}^*] = \begin{bmatrix} [A_d] & [B_d] \\ 0 & I \end{bmatrix} \tag{2.67}$$

$$[{C_d}^*] = [[C_d] \quad [0]_{mxn}] \tag{2.68}$$

For the Augmented Kalman Filter algorithm, prediction phase:

$$\{x^*\}_k^- = [{A_d}^*]\{x^*\}_{k-1}^+ \tag{2.69}$$

$$[P]_k^- = [{A_d}^*][P]_{k-1}^+[{A_d}^*]^T + [Q^*] \tag{2.70}$$

Update phase:

$$\{z\}_k = \{y\}_k - [{C_d}^*]\{x^*\}_k^- \tag{2.71}$$

$$[K_k] = [P]_k^-[{C_d}^*]^T([R] + [{C_d}^*][P]_k^-[{C_d}^*]^T)^{-1} \tag{2.72}$$

$$\{x^*\}_k^+ = \{x^*\}_k^- + [K]_k[z]_k \tag{2.73}$$

$$[P]_k^+ = ([I] - [K]_k[{C_d}^*])[P]_k^- \tag{2.74}$$

Dimensions of these matrixes are as follows:

$\{x^*\}$: 3n x 1,

$\{y\}$: m x 1,

$[{A_d}^*]$: 3n x 3n,

$[{C_d}^*]$: m x 3n,

$[P]$: 3n x 3n,

$[Q^*]$: 3n x 3n,

$[R]$: m x m,

$[K]$: 3n x m,

$\{z\}$: m x 1.

Where:

$$[Q^*] = \begin{bmatrix} Q & 0 \\ 0 & S \end{bmatrix} \tag{2.75}$$

And S is the covariance of load reoccurrence noise.

When an Augmented Kalman Filter is used, forces will be one of the outputs of the process. Which then can be immediately signal processed in order to obtain unbalance masses. On the other hand, there is a problematic situation here related with the nature of unbalance forces. This application is suitable for structural dynamics in general, but since unbalance forces are changing direction and have sinusoidal characteristics, the current state introduces a huge convergence problem. That is, the Augmented Kalman Filter will try to obtain an outdated force value at each time step. This requires further modifications to the formulation in order to obtain convergence.

2.4.4 Further modifications on formulation

As explained, the current formulation introduces a huge convergence problem to the study as unbalance forces are time-dependent. One clever way of avoiding this problem is; that instead of setting unbalance forces as a state, let unbalance be a system state. This way, with some additional modifications to the formulation by also keeping the nature of the problem all the same, the Augmented Kalman Filter will target fixed values of unbalance instead of time-dependent force values.

Note that unbalance forces are in the form [18]:

$$f(t) = \begin{cases} U\omega^2 \cos(\omega t + \varphi) \\ U\omega^2 \sin(\omega t + \varphi) \end{cases} \tag{2.76}$$

This means these can be expressed in a generalized manner such as;

$$\{f(t)\}_{nx1} = \omega^2 [F(\omega t)]_{nxn} \{U\}_{nx1} \tag{2.77}$$

It should also be mentioned that:

$$U\cos(\omega t + \varphi) = U_x \cos(\omega t) + U_y \sin(\omega t) \tag{2.78}$$

$$U\sin(\omega t + \varphi) = U_x \sin(\omega t) - U_y \cos(\omega t) \tag{2.79}$$

$$U = \sqrt{{U_x}^2 + {U_y}^2} \tag{2.80}$$

$$\varphi = \tan^{-1} \frac{-U_y}{U_x} \tag{2.81}$$

Thus, one can write the expression;

$$\{f(t)\} = \omega^2 \begin{bmatrix} \cos(\omega t) & \sin(\omega t) & 0 & 0 \\ \sin(\omega t) & -\cos(\omega t) & 0 & 0 \\ 0 & 0 & 0 & 0 \\ 0 & 0 & 0 & 0 \end{bmatrix} \begin{bmatrix} U_x \\ U_y \\ 0 \\ 0 \end{bmatrix} \tag{2.82}$$

Now note that the force expression is decomposed into time or speed-dependent terms and unbalance values. The purpose of the whole study is to obtain values U and φ. Now that these values can be derived easily using vector $\{U\}$. So, the whole formulation must be modified so that $\{U\}$ is a state vector and other matrix definitions are in correlation with this update.

Input (2.77) into (2.51) and rewrite to get state space representation with unbalances:

$$\{x\}_k = [A_d]\{x\}_{k-1} + [B_d]\omega^2 [F(\omega t)]_{k-1} \{U\}_{k-1} \tag{2.83}$$

$$\{y\}_k = [C_d]\{x\}_k \tag{2.84}$$

Let new state vector for Augmented Kalman Filter be:

$$\{x^a\} = [\{x\}\,\{\dot{x}\}\,\{U\}]^T \tag{2.85}$$

New Augmented Kalman Filter space state representation:

$$\{x^a\}_k = [\Psi]\{x^a\}_{k-1} \tag{2.86}$$

$$\{y\}_k = [\mathrm{H}]\{x^a\}_k \tag{2.87}$$

Where:

$$[\Psi] = \begin{bmatrix} [A_d] & [\Gamma] \\ 0 & I \end{bmatrix} \tag{2.88}$$

$$[\Gamma] = \omega^2[B_d][F(\omega t)]_{k-1} \tag{2.89}$$

$$[\mathrm{H}] = [[C_d] \quad 0] \tag{2.90}$$

The rest of the formulation is in general Augmented Kalman Filter form; prediction phase:

$$\{x^a\}_k^- = [\Psi]\{x^a\}_{k-1}^+ \tag{2.91}$$

$$[P]_k^- = [\Psi][P]_{k-1}^+[\Psi]^T + [Q^*] \tag{2.92}$$

Update phase:

$$\{z\}_k = \{y\}_k - [\mathrm{H}]\{x^a\}_k^- \tag{2.93}$$

$$[K_k] = [P]_k^-[\mathrm{H}]^T([R] + [\mathrm{H}][P]_k^-[\mathrm{H}]^T)^{-1} \tag{2.94}$$

$$\{x^a\}_k^+ = \{x^a\}_k^- + [K]_k[z]_k \tag{2.95}$$

$$[P]_k^+ = ([I] - [K]_k[\mathrm{H}])[P]_k^- \tag{2.96}$$

At this point, finally, unbalance components in both directions are obtained. As explained before, these components will also help identify the phase angle as well.

2.5 Balancing Conditions

Now that the unbalance values are obtained using measurement data, the only step left to take is setting the balancing conditions. It was shared before that the Kalman Filter will be using a direct formulation and balancing conditions will be set using a modal approach.

Up to this point, the gyroscopic effect was taken into account for all the calculations. For the common modal balancing approach and its conditions, mode shapes obtained with only inertia and stiffness matrixes are used. Instead, it is not hard to set almost identical conditions by also taking into account the gyroscopic effect. According to the modal balancing theory, in order to balance a rotating shaft; one should balance the current mode by not disturbing the prior balanced modes. Mathematical expressions for these conditions are as [4]:

Balance the N^{th} mode;

$$\sum_{k=1}^{n} m_k \overline{a_k} \phi_N(x_k) = -m_N \overline{a_N} \tag{2.97}$$

Here, eccentricity values a are complex numbers in order to take into account both directions.

Do not disturb the earlier balanced modes;

$$\sum_{k=1}^{n} m_k \overline{a_k} \phi_u(x_k) = 0 \quad for \quad u = 1,2,\dots,N-1 \tag{2.98}$$

We can modify these expressions to better fit to the balancing method being proposed in this study. It was stated that using the Kalman Filter formulation, it is possible to obtain unbalance values as well as phase angles of the unbalance masses. One more point that should be reminded is that, in our case, mode shapes are speed-dependent.

From the modal theory; it is known that at the first critical speed, the system response will be almost identical to the first mode that critical speed belongs to. As one approaches to higher critical speeds, lower modes will have a considerable contribution to that mode, but higher modes' contribution will be significantly less,

which will be enough to neglect. As a procedure, it is possible to isolate the first mode and obtain the modal unbalance value. Then, by readjusting the expressions on top to consider the gyroscopic effect, it is possible to balance this first mode. Also, the eccentricity value could be expressed as:

$$\bar{a} = ae^{-i\varphi} \tag{2.99}$$

So, for isolated modes, Kalman Filter should provide:

$$m_N\overline{a_N} = U_N e^{-i\varphi_N} \tag{2.100}$$

Since the mode shapes are speed-dependent, balancing conditions must be set for critical speed points. One more remark is that the above formulation is for continuous rotors. So, the mode shapes are vectors of axial position. In our case, the rotor is discrete and one should take into account the nodal positions. Now rephrase the balancing condition as:

Balance the N^{th} mode;

$$\sum_{k=1}^{n} m_k a_k e^{-i\varphi_k}\phi_N(x_k)|_{\omega=\omega_{cr,N}} = -U_N e^{-i\varphi_N} \tag{2.101}$$

Do not disturb the earlier balanced u^{th} mode;

$$\sum_{k=1}^{n} m_k a_k e^{-i\varphi_k}\phi_u(x_k)|_{\omega=\omega_{cr,u}} = 0 \quad ; \quad u = 1,2,\dots,N-1 \tag{2.102}$$

2.6 Newmark Algorithm

A method is required to be used during numerical calculations as a numerical solver, to generate simulation data. Research on the literature revealed that the Newmark Algorithm is a widely used structural dynamics integrator that can accommodate the nonlinear effects as well. It is useful to implement a solver that can accommodate nonlinear effects since the gyroscopic matrix is speed-dependent. When the speed scenario is non-constant, this system's behavior is nonlinear.

Newmark Algorithm can be summarised as below [19]:

$$\ddot{x}_0 = [M]^{-1}([G]\dot{x}_0 + [K]x_0) \tag{2.103}$$

Where;

x_0: Initial displacement,

$\dot{x}_0$: Initial velocity.

Update at each time step for nonlinearity:

$$\left[\widehat{K}\right] = [K] + a_0[M] + a_1[G(\omega)] \tag{2.104}$$

Time stepping part:

$$\begin{aligned}\left\{\widehat{F}\right\}_{t+\Delta t} = \{F\}_{t+\Delta t} + [M](a_0 x_t + a_2\dot{x}_t + a_3\ddot{x}_t) \\ + [G(\omega)](a_1 x_t + a_4\dot{x}_t + a_5\ddot{x}_t)\end{aligned} \tag{2.105}$$

$$x_{t+\Delta t} = \left[\widehat{K}\right]^{-1}\left\{\widehat{F}\right\}_{t+\Delta t} \tag{2.106}$$

$$\ddot{x}_{t+\Delta t} = a_0(x_{t+\Delta t} - x_t) - a_2\dot{x}_t - a_3\ddot{x}_t \tag{2.107}$$

$$\dot{x}_{t+\Delta t} = \dot{x}_t + a_6\ddot{x}_t + a_7\ddot{x}_{t+\Delta t} \tag{2.108}$$

Here;

$$a_0 = \frac{1}{\alpha\Delta t^2} \;\; ; \;\; a_1 = \frac{\delta}{\alpha\Delta t} \;\; ; \;\; a_2 = \frac{1}{\alpha\Delta t} \;\; ; \;\; a_3 = \frac{1}{2\alpha} - 1 \tag{2.109}$$

$$a_4 = \frac{\delta}{\alpha} - 1 \;\; ; \;\; a_5 = \frac{\Delta t}{2}\left(\frac{\delta}{\alpha} - 2\right) \;\; ; \;\; a_6 = \Delta t(1-\delta) \;\; ; \;\; a_7 = \delta\Delta t \tag{2.110}$$

And;

Δt: Time step,

$\alpha = 0{,}25$,

$\delta = 0{,}5$.

3. NUMERICAL AND EXPERIMENTAL STUDIES

3.1 Numerical Studies

Here in this section, a simple example problem will be created virtually and the above formulation will be applied. MATLAB and ANSYS are the engineering tools to be taken help from. This is done prior to doing field balancing studies.

3.1.1 Definition of the system

Assume an elastic shaft with two discs mounted on known locations. A representation of the elastic shaft can be seen in Figure 3.1. The shaft has a constant solid circular cross-section with 2,5 mm, and its length is 200 mm. The material of the elastic shaft is steel and has the properties in Table 3.1. There are two mounted discs that are unbalanced. These unbalance values will be defined in the latter sections. The shaft is mounted into bearings at each end.

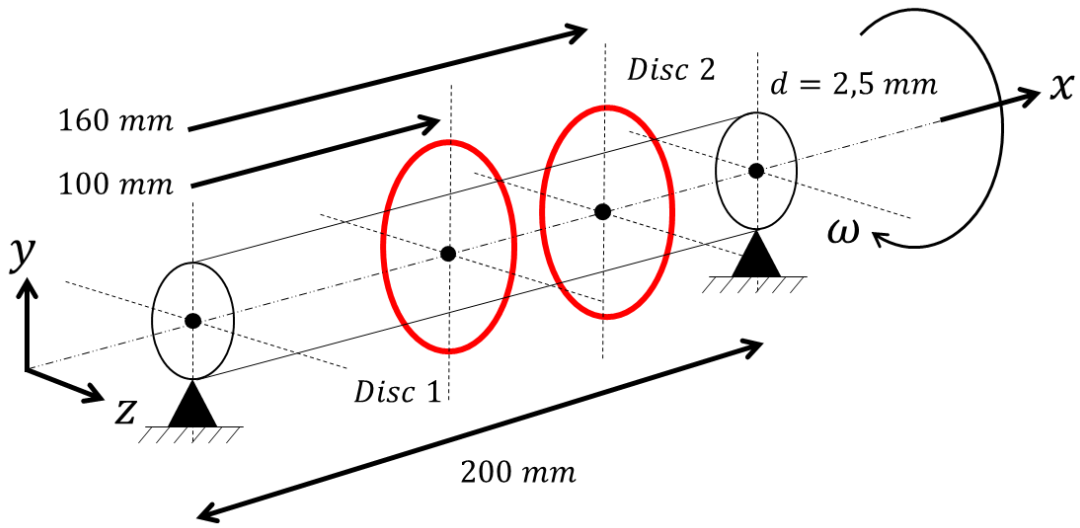

Figure 3.1: Virtual eccentric shaft problem.

A MATLAB code was written to handle the calculations that will be done in this section. The system is modeled using the 1D Euler-Bernoulli Beam Theory. The total length of 200 mm is divided into 100 elements, with each having 2 mm of length.

Formulation shared on (2.18) - (2.24) is used to create the FE model. Discs are modeled as 1D point masses at defined locations.

Table 3.1: Material properties of the elastic shaft.

Property	Value
Material	Steel
Density	7850 kg/m^3
Modulus of Elasticity	200 GPa
Shear Modulus	80 GPa
Poisson's Ratio	0,3

3.1.2 Eigenvalue solution

Since the balancing approach described in the study is a modal approach, the first study to be made should be obtaining modal properties. A check is made between MATLAB and ANSYS to make sure modal properties are similar. ANSYS is also used to generate a Campbell Diagram so that the critical speeds are identified.

Modal analysis is made on MATLAB as well as ANSYS. Natural frequencies obtained for the first five modes from MATLAB can be seen in Figure 3.2.

	1
1	123.8854
2	123.8854
3	495.5449
4	495.5449
5	1.1150e+03
6	1.1150e+03
7	1.9824e+03
8	1.9824e+03
9	3.0979e+03
10	3.0979e+03

Figure 3.2: First five natural frequencies obtained from MATLAB.

Modal analysis results obtained from ANSYS can be seen in Figure 3.3. If the results are compared, it can be stated that there is a very high correlation between the results and the modeling done on MATLAB is also very accurate based on a widely used commercial structural analysis program.

Tabular Data

	Set	Solve Point	Mode	Damped Frequency [Hz]
1	1,	1,	1,	0,
2	2,	1,	2,	123,78
3	3,	1,	3,	123,78
4	4,	1,	4,	494,84
5	5,	1,	5,	494,84
6	6,	1,	6,	1112,3
7	7,	1,	7,	1112,3
8	8,	1,	8,	1974,8
9	9,	1,	9,	1974,8
10	10,	1,	10,	3080,2
11	11,	1,	11,	3080,2

Figure 3.3: First five natural frequencies obtained from ANSYS.

The next step is to obtain the Campbell Diagram using ANSYS. This is useful for identifying critical speeds of the rotating hardware. The Campbell Diagram of the system can be seen in Figure 3.4.

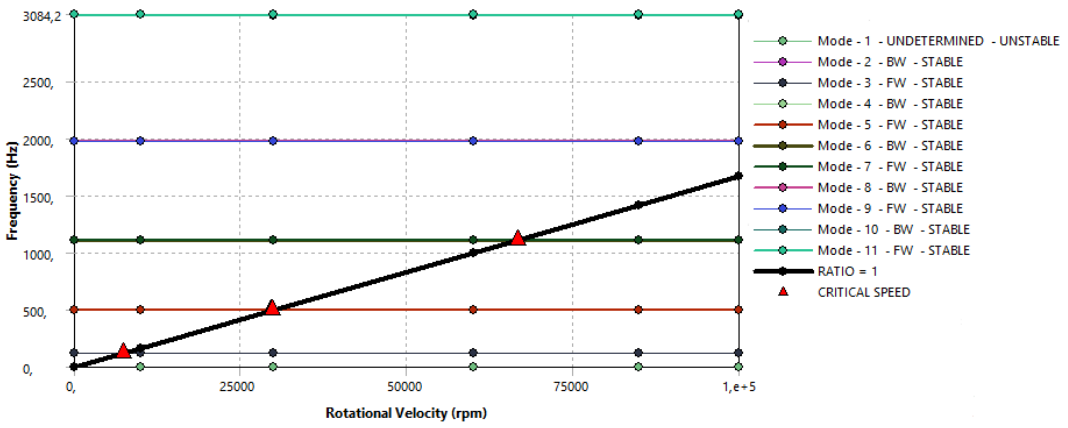

Figure 3.4: Campbell Diagram of the rotating hardware.

According to the results, critical speeds are as in Table 3.2. These critical speeds are first-engine order critical speeds since it is the cause of unbalance excitation. The analysis is made up to 100000 rpm speed.

Table 3.2: Critical speed map of the rotating hardware.

Mode	Whirl Direction	Critical Speed
1	Undetermined	0 rpm
2	BW	7426,2 rpm
3	FW	7427,6 rpm
4	BW	29679 rpm
5	FW	29702 rpm
6	BW	66681 rpm
7	FW	66796 rpm

3.1.3 Forced vibration solution

Now that the system is validated via a commercial FEM program, it is ready to be run in a MATLAB environment. Since this is a virtual example, a numerical solver is necessary to be implemented into MATLAB code. The numerical solver will take system matrixes, speed scenarios, time steps and unbalance inputs and use them to create time domain responses for displacements, velocities and accelerations.

It is decided to run the system for 5 seconds at a constant rotational speed. This constant rotational speed is taken as 6690 rpm, which is around 90% of the first critical speed. The reason behind taking this value is; that it was stated before that during the balancing process, the data will be collected at speeds that are close to critical speeds. Under these circumstances, the response of the system will be almost identical to the first mode.

The system is set to be at rest for the initial conditions where there is neither initial displacement nor initial velocity. So, care should be taken when post-processing the values at early time steps. This is because the whole scenario is a fixed rotational speed case and first-time steps will be enforcing the system into an unrealistic motion.

The unbalance value defined at the Disc 1 location is 0.02 kg.m and the unbalance value at Disc 2 is 0.04 kg.m. Using these values, the forcing matrix is formed with the relation (2.6) - (2.7) prior to running Newmark Algorithm. This forcing matrix is used as an input for the Newmark Algorithm. The time step is set to 0,0001 s so that the sampling rate is 10000 Hz. The summary of the analysis options is in Table 3.3.

Table 3.3: Analysis options provided for MATLAB code.

Option	Set To
Solver	Newmark
Analysis Time	5 s
Time Step	0,0001 s
Sampling Rate	10000 Hz
Rotational Speed	6690 rpm

The analysis had run and displacement, velocity and acceleration outputs for each nodal position were obtained. Some of the outputs are shared as below. At a random time, such as time step 36924, which corresponds to t=3,36923 s, has the shaft deflection shape, which can be seen in Figure 3.5.

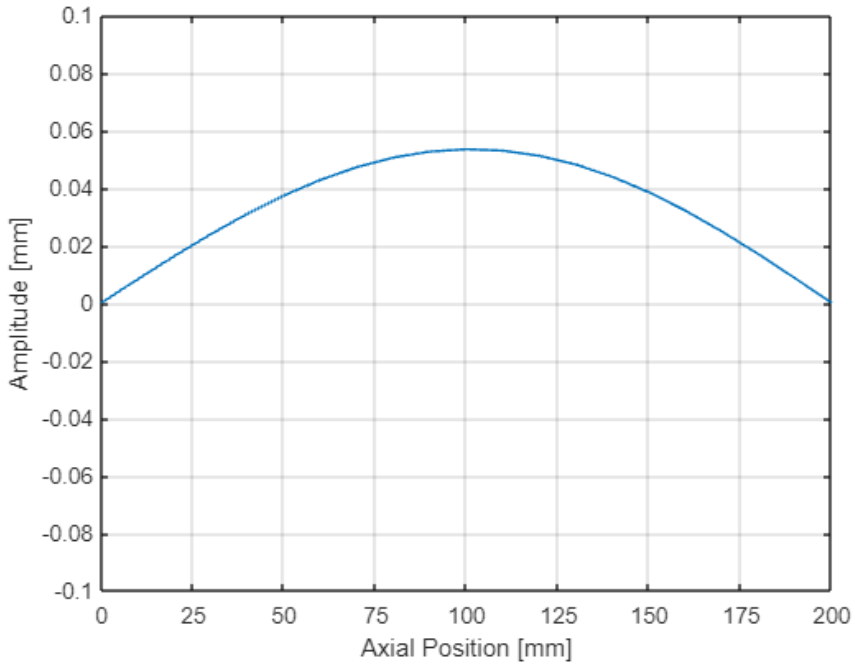

Figure 3.5: Shaft deflection on y-direction at time t=3,36923 s.

The system response of node number 70, which corresponds to axial position of 140 mm, is shared in Figure 3.6 for full time span of the analysis.

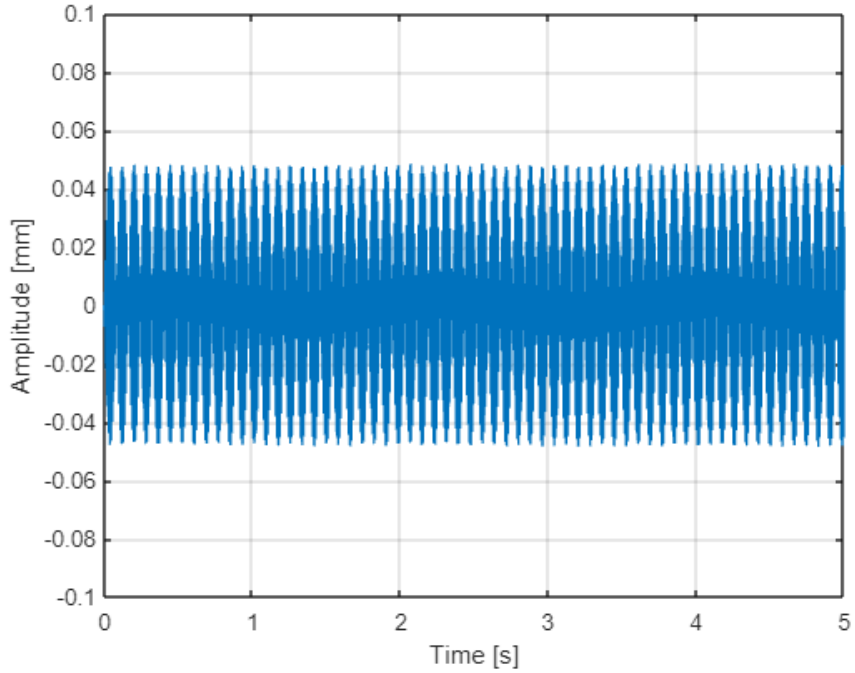

Figure 3.6: Response of the node 70 on y-direction for full time span.

In the Figure 3.7, the response of node number 70 is shared again for a time span in between t=4,5 s and t=5 s.

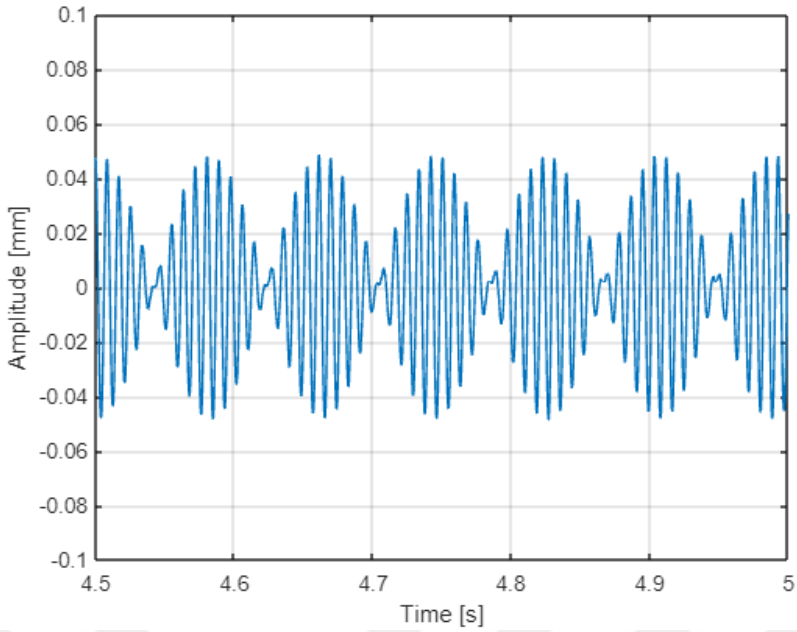

Figure 3.7: Response of the node 70 on y-direction for time span in between t=4,5 s and t=5 s.

3.1.4 Kalman Filter

Obtained displacement time domain solution from the Newmark Algorithm will be used to feed to the Augmented Kalman Filter that was described in the previous sections. In order to reflect a more realistic scenario, the number of fed linear displacement DoFs will be limited to 6, where there are 202 linear displacement DoFs in the system. This means it is assumed that there are displacement sensors at 3 different locations, which are measuring at both the y-axis and z-axis. Let these sensors be at axial positions 50 mm, 110 mm and 180 mm. A schematic for such a case can be seen in Figure 3.8.

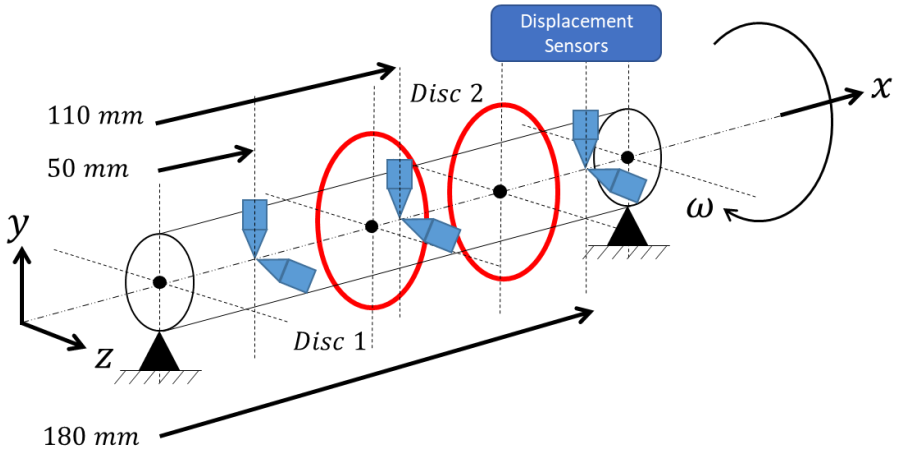

Figure 3.8: Schematic for displacement sensor positions.

Some definitions for the Kalman Filter algorithm were made in the earlier sections, such as covariance matrixes. Input values for these matrixes can be found in Table 3.4.

Table 3.4: Kalman Filter inputs.

Input	Value
Process Noise Covariance	10
Measurement Noise Covariance	1
Initial Error Covariance	1

Results of the Newmark Algorithm are fed to the Kalman Filter and the algorithm was run using MATLAB. Kalman Filter estimates the displacement, velocity, acceleration and unbalance values for unknown locations with the help of measurement data.

3.1.5 Numerical results

As explained, results are obtained from the Kalman Filter. Now, the Kalman Filter results will be compared with Newmark Algorithm results. The real case, which was obtained from the Newmark Algorithm and Kalman Filter estimated comparison of shaft deflection shape at a random time step 48445, which corresponds to t=4,8444 s, can be seen in Figure 3.9.

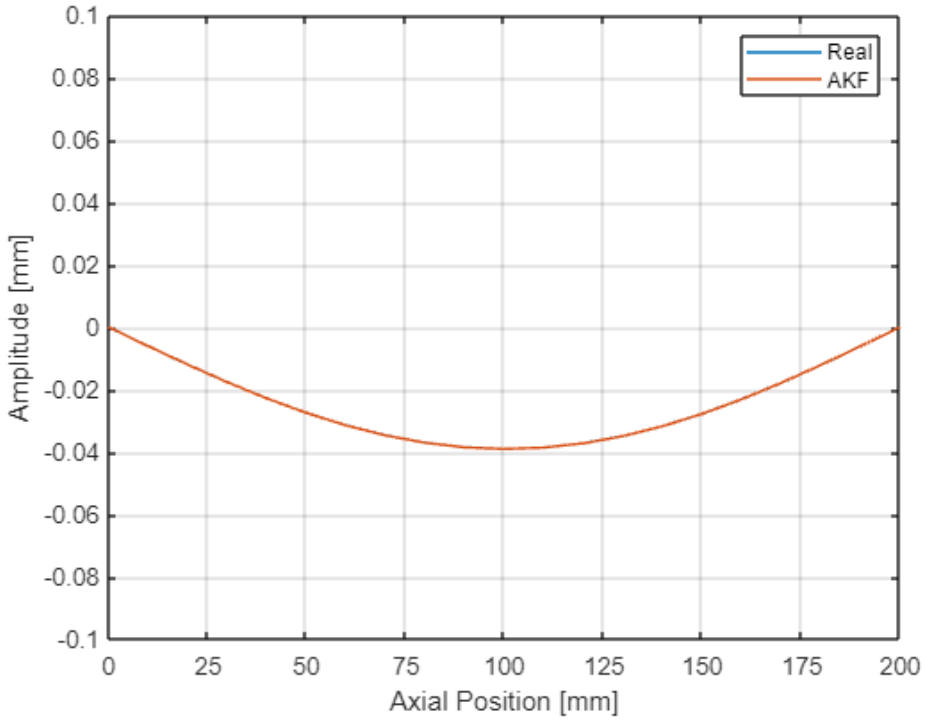

Figure 3.9: Shaft deflection comparison generated by Newmark Algorithm and Kalman Filter on y-direction at time t=4,8444 s.

As can be seen from Figure 3.9, the difference between the two different data is not much visible. In order to notice the difference between the two data, a closer look at the point around the axial position 200 mm can be found in Figure 3.10; one can understand from this figure that the error is around 10^{-5} mm level which is very accurate for such a hard task.

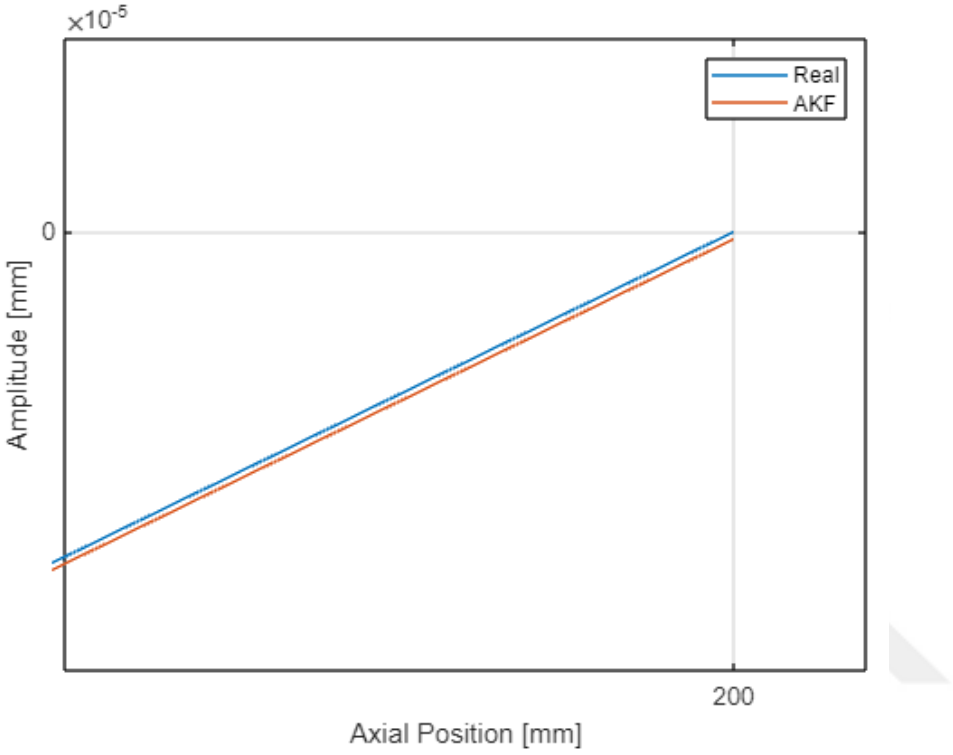

Figure 3.10: Closer look around axial position 200 mm at t=4,8444 s.

The next point to compare is the unbalance forces. As can be seen from Figure 3.11, unbalance forces generated by the Kalman Filter are very accurate but have a high-frequency noise-like effect on the data. This is highly due to parameters introduced in Table 3.4 which determines the performance of the Kalman Filter. These values can make the Kalman Filter to be more biased towards measurement data or analytical models depending on the values. But looking at the perspective of the current data comparison in Figure 3.11, with the usage of a low-pass filter, this high-frequency noise-like effect can be removed. Estimated data is very accurate at following the profile of real data as well as estimating the time lag.

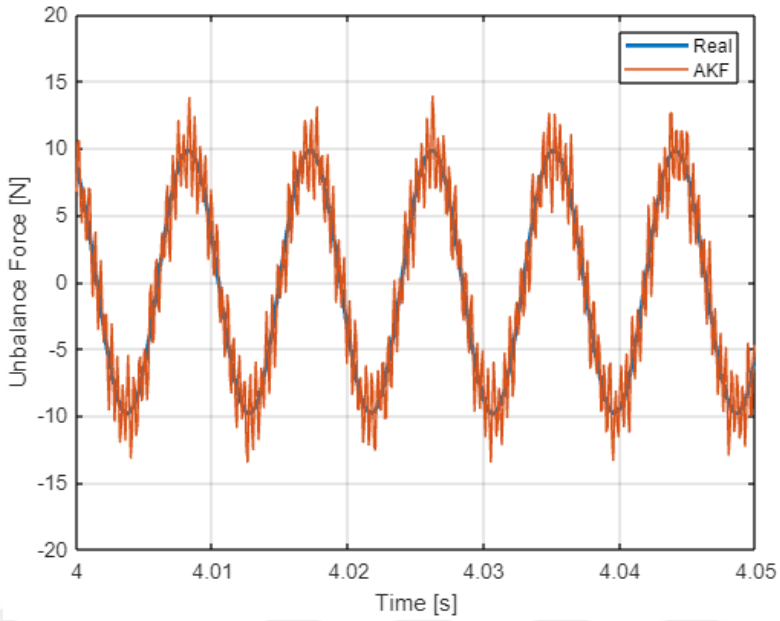

Figure 3.11: Unbalance force comparison generated by Newmark Algorithm and Kalman Filter on y-direction for Disc 1.

The final value to check is the unbalance values. This is the most important step since the main focus of this study is balancing and the whole formulation had been prepared targeting to accurately obtain unbalance values. It was stated before that the unbalance values defined for Disc 1 and Disc 2 were 0.02 kg.m and 0.04 kg.m, respectively. One can see from Figure 3.12 that unbalance estimations of the Kalman Filter had been fluctuating around the exact value during the whole data processing. The result is very promising and could be improved by some iterations for the values in Table 3.4.

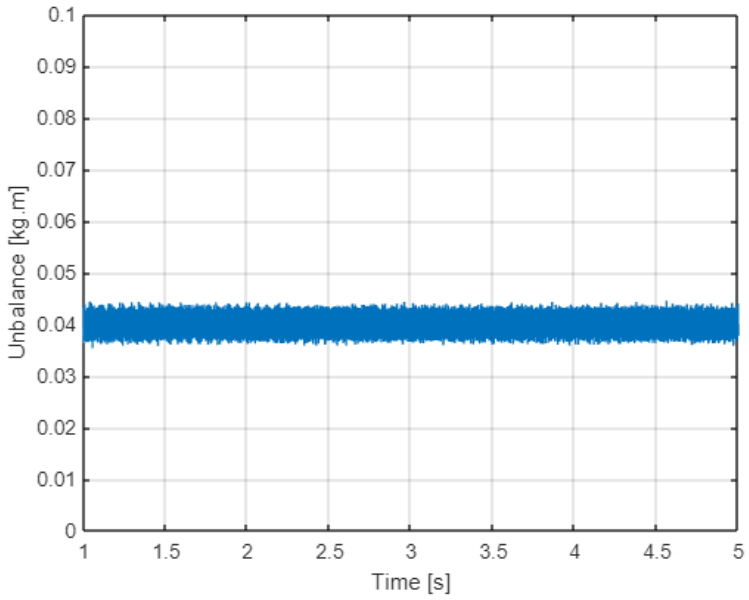

Figure 3.12: Unbalance value estimation generated by Kalman Filter for Disc 2.

3.2 Experimental Studies

This section will include an experimental balancing case. A test rig that is created for balancing purposes is used. The test rig will be explained in detail. Data gathered from the rig and above explanations and formulations are used to solve the problem. In the process, Hypermesh, Abaqus and MATLAB are used as the engineering tools.

3.2.1 Test rig and setup

As mentioned above, the used rig is a dedicated test rig for balancing purposes. Figure 3.13 can be seen, as well as the coordinate system. As can be understood, there is a shaft mounted to bearings at locations close to its ends. The origin of the setup is picked to be the rightmost end of the shaft. The shaft has 4 discs mounted on it and is connected to an electric motor via a flexible coupling on the rightmost end. The discs are named as in Figure 3.13.

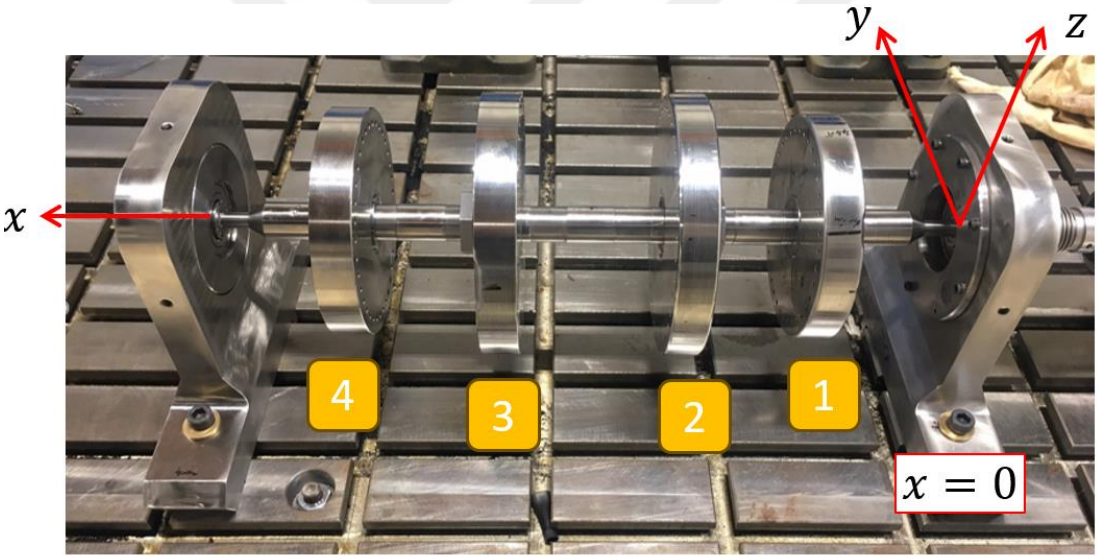

Figure 3.13: Test setup used for balancing calculations.

The density of the material of the shaft is 8220 kg/m^3 and the modulus of elasticity is 203 GPa. A schematic view of the cross-sectional properties of the shaft is provided in Figure 3.14. Dimensions provided in this figure are in millimeters.

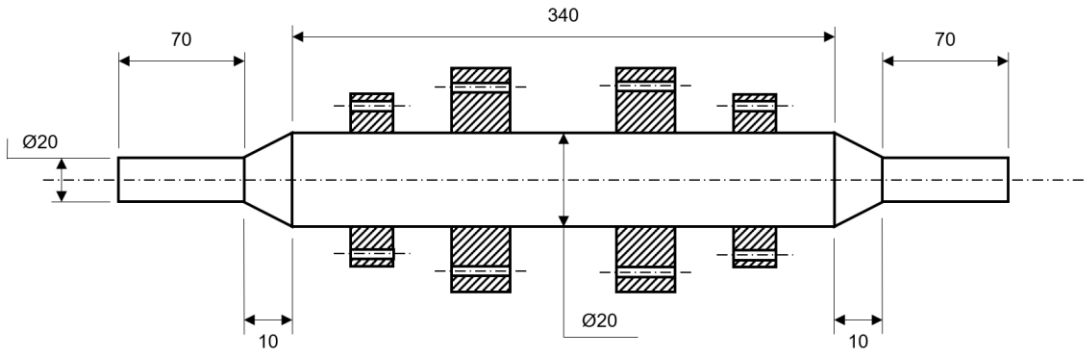

Figure 3.14: Dimensional properties of the shaft.

The shaft is mounted on its bearings, 20 mm inwards from its ends. The inertial properties of discs are provided in Table 3.5.

Table 3.5: Inertial properties of the discs mounted on the shaft.

Disc	Mass	Diametral Inertia	Polar Inertia
1	1.739 kg	0.001634 kg.m^2	0.003135 kg.m^2
2	2.386 kg	0.003009 kg.m^2	0.005842 kg.m^2
3	2.386 kg	0.003009 kg.m^2	0.005842 kg.m^2
4	1.739 kg	0.001634 kg.m^2	0.003135 kg.m^2

3.2.2 FE model creation and validation

As explained in the previous sections, the application of the Kalman Filter formulation requires a physical model as an input as well as the test data.

Considering the information provided above, a 1D FE model is created using Hypermesh. Since this is a 1D model, beam formulations are followed for the shaft and discs are modeled as the point masses. Later on, the mesh file is exported from Hypermesh into Abaqus. This is done in order to obtain mass and stiffness matrixes from Abaqus.

The gyroscopic matrix is created using MATLAB by considering the equations (2.21) and (2.24). The reason for creating the gyroscopic matrix by hand calculation is Abaqus does not have the capability to export the gyroscopic matrix.

The created model has 5 mm of elemental length, which means the model has 100 elements, 101 nodes and 404 DoFs.

The Campbell Diagram of the test setup is provided by the test rig team, which is as in Figure 3.15. The model validation is done by using the data in this diagram.

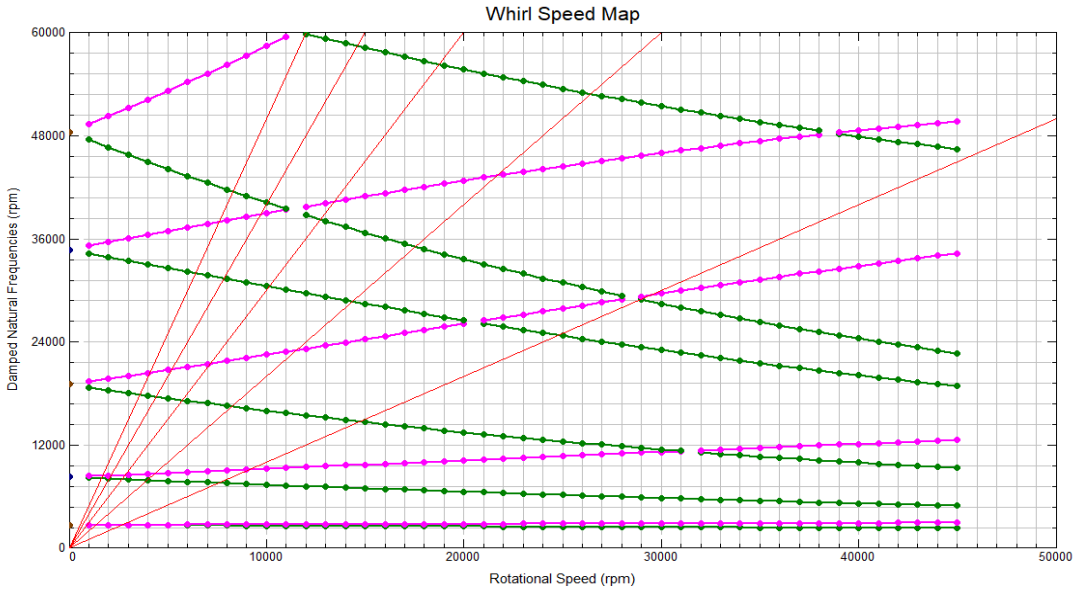

Figure 3.15: Campbell Diagram of the test rig.

Obtained system matrixes are imported into the MATLAB environment. Fixed boundary conditions are applied at bearing locations and a standstill modal analysis is carried out for model validation purposes. Obtained results from the MATLAB are shared in Figure 3.16.

	1
1	47.6843
2	47.6843
3	154.4832
4	154.4832
5	337.9016
6	337.9016
7	594.4494
8	594.4494
9	813.3514
10	813.3514

Figure 3.16: Standstill natural frequencies obtained from MATLAB.

Using the information on the Campbell Diagram in Figure 3.15 and results obtained in Figure 3.16, a summary and model validation table is created as in Table 3.6. It can be

stated that, the FE model's accuracy is at a reasonable level and can be used for Kalman Filter calculations.

Table 3.6: Standstill natural frequency comparison.

Mode	Campbell Diagram	MATLAB	Difference
1	48 Hz	47.68 Hz	-0.7 %
2	140 Hz	154.48 Hz	+10.3 %
3	316.67 Hz	337.90 Hz	+6.7 %
4	580 Hz	594.45 Hz	+2.5 %
5	808 Hz	813.35 Hz	+0.7 %

3.2.3 Test scenario and obtained data

According to the Campbell Diagram in Figure 3.15, it is possible to say that the first critical speed is around 2950 rpm. In that case, a test decided to be carried out at a fixed speed, which is desired to be as close as possible to 2950 rpm.

According to the definitions made in the previous chapters, the theory of application requires displacement data as an input. During the test, Eddy Current Sensors, which are capable of measuring very low displacement at a very high accuracy, are used. One important piece of information that has to be provided is the test rig team has only 4 Eddy Probes. The intention is to provide as much displacement data as possible to the Kalman Filter so that it has a better convergence. Eddy Probes have to be positioned in lateral directions and with a 90° angle to each other. Under these circumstances, it is only possible to gather data from 2 different discs. In that case, two different tests decided to be run by keeping one of the instrumentation locations the same and changing the other. In that manner; gathered data can be postprocessed and by considering the reference disc, it is possible to use these data together and take them as carried on the same test. The sampling rate of the collected data is 1600 Hz.

The first test is run with the instrumentation that can be seen in Figure 3.17. On this plan, Disc 4 is used as the reference disc and instrumentation at this disc was kept the same on the second run as well. Two other probes are placed to measure the data from Disc 3.

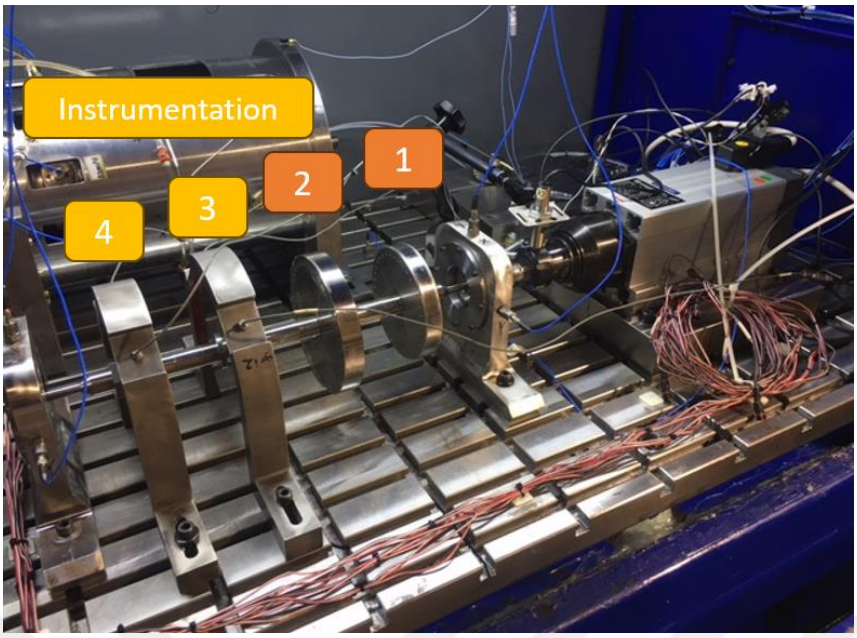

Figure 3.17: Instrumentation configuration, first test.

The configuration of the second run can be seen in Figure 3.18. As explained, Disc 4 is the reference disc and on this second run, data is gathered from Disc 2.

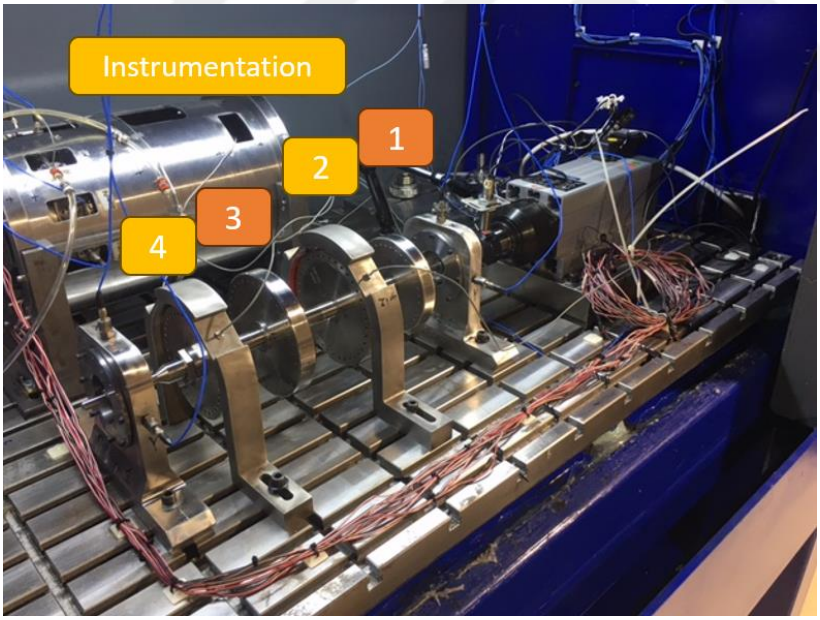

Figure 3.18: Instrumentation configuration, second test.

The speed scenario of the tests can be seen in Figure 3.19. During the runs, it was found that the test system could run in a stable manner at rotational speeds around 3270 rpm. So, during both tests, the system is brought to 3270 rpm and kept at this speed for a certain amount of time. Only the data generated around this speed region is used during the balancing calculations.

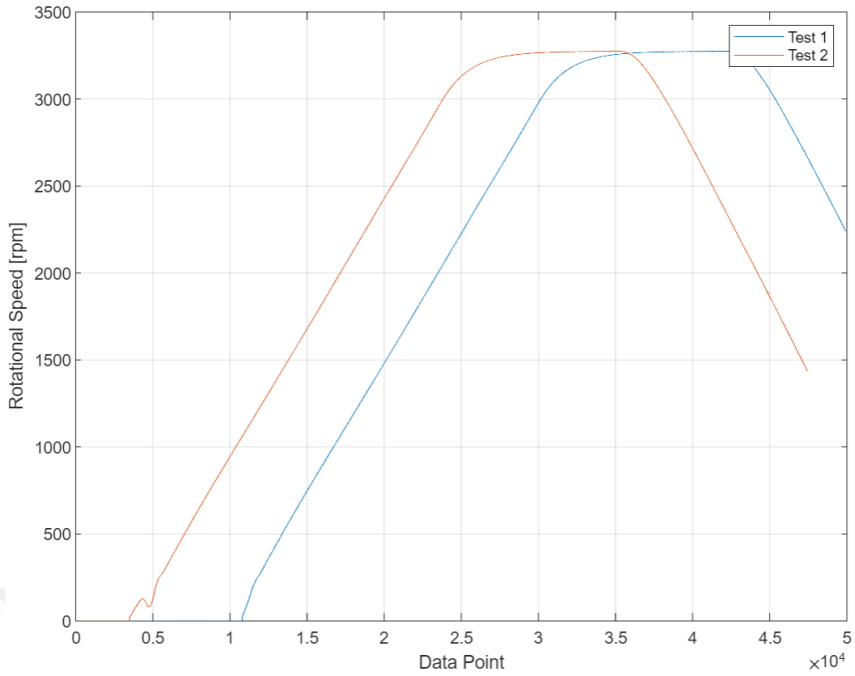

Figure 3.19: Speed information of the two test runs.

Test 1 signal is taken as a reference to post-process the Test 2 signals so that the reference angle of the two tests are the same. Using the reference disc data, which is Disc 4, Disc 2 data is adjusted. The accuracy of the adjustment can be seen in Figure 3.20. Since this is digital data, it is not possible to obtain 100 % precision. In the final case, accuracy is less than one data point interval, which is 0.000625 s.

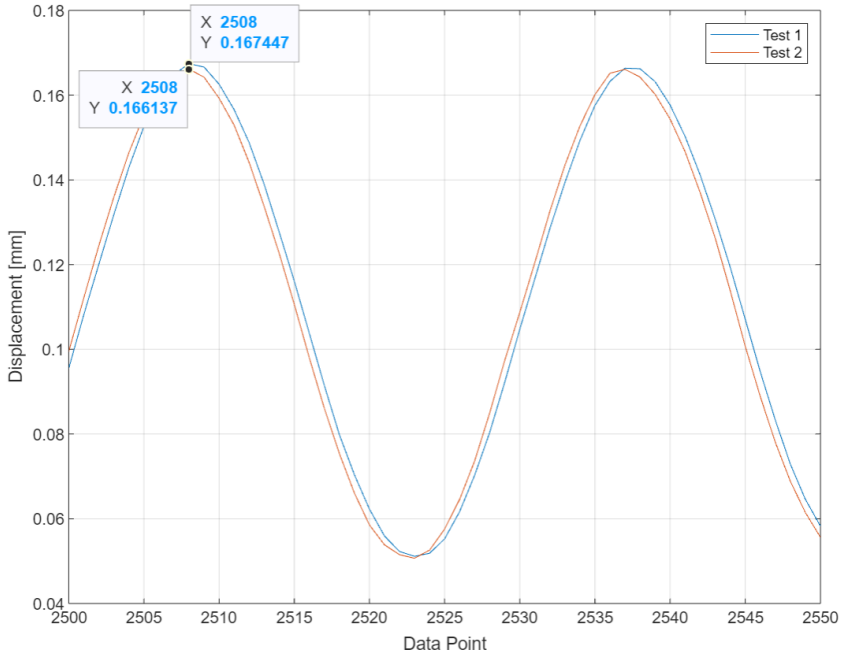

Figure 3.20: Accuracy of the adjusted data.

As the final inputs for the Kalman Filter, a portion of the obtained Disc 2 displacements can be seen in Figure 3.21. DoF and node numbers are shared in the legend section. DoF 161 is the displacement in the Y direction and DoF 162 is the displacement in the Z direction.

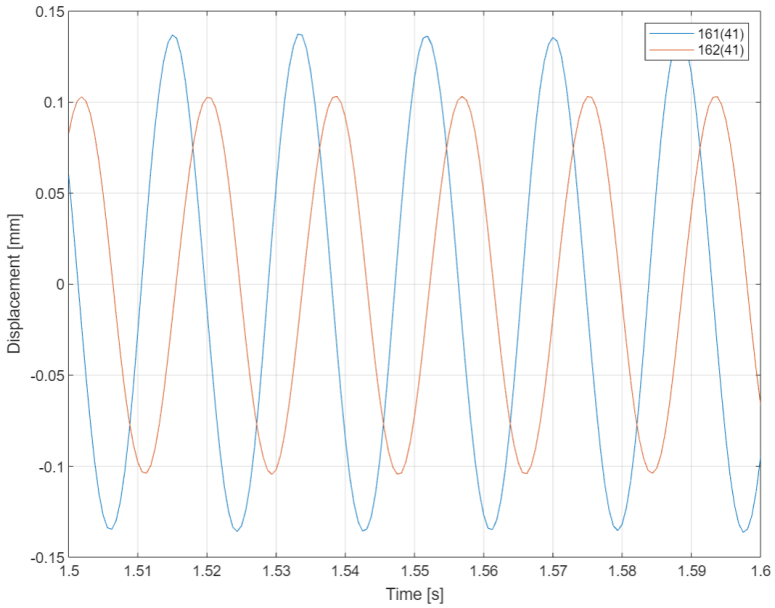

Figure 3.21: A portion of Disc 2 input for Kalman Filter.

Disc 3 input for the Kalman Filter is as shared in Figure 3.22. DoF and node numbers are, again, shared in the legend section. DoF 241 is the displacement in the Y direction and DoF 242 is the displacement in the Z direction.

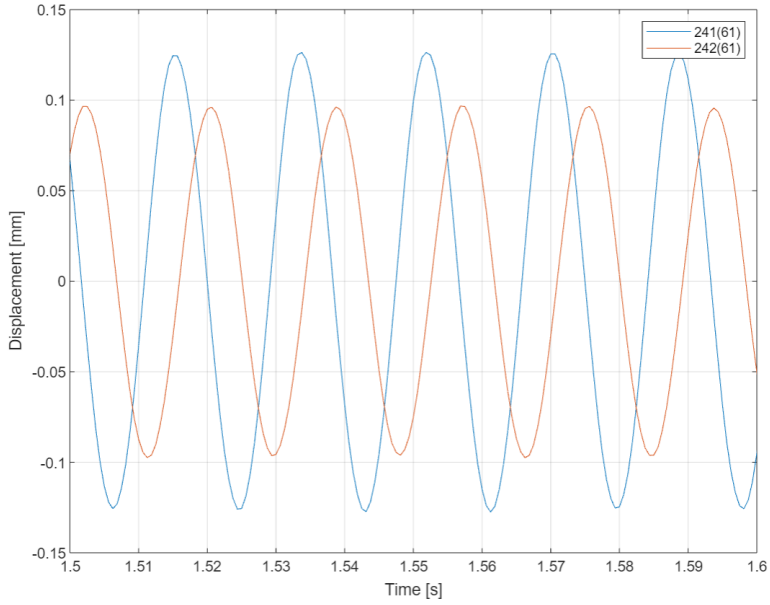

Figure 3.22: A portion of Disc 3 input for Kalman Filter.

Disc 4 input can be observed in Figure 3.23. DoF 301 is the displacement in the Y direction and DoF 302 is the displacement in the Z direction.

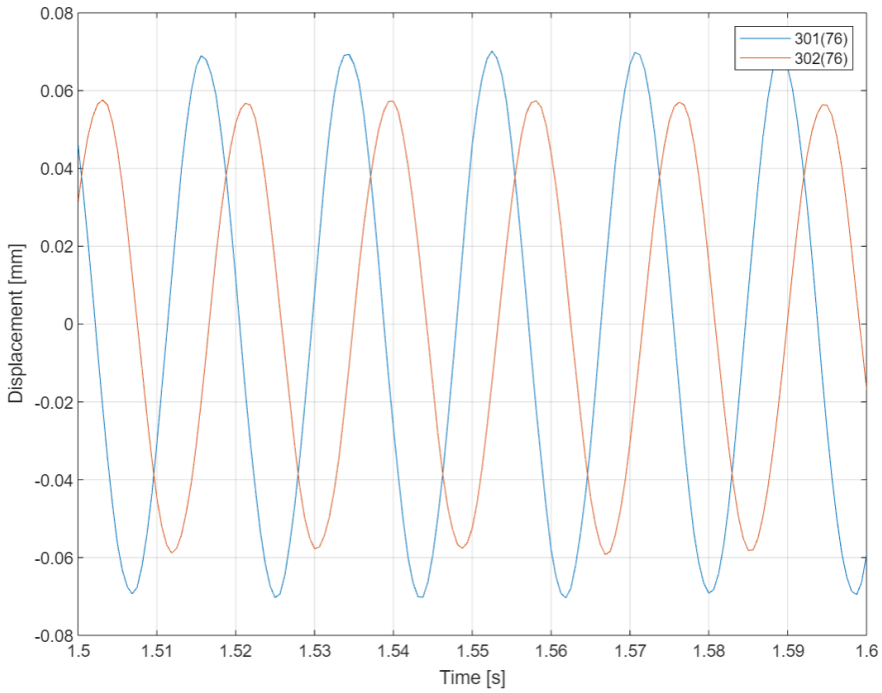

Figure 3.23: A portion of Disc 4 input for Kalman Filter.

These displacement values, as well as the rotational speed history of the system, are fed to the Kalman Filter calculations.

3.2.4 Balancing calculations

It is decided to do balancing, initially on the MATLAB environment. For that reason, the Kalman Filter Algorithm is run to obtain initial unbalance values. These values are defined in the MATLAB environment again to run a Newmark Algorithm to regenerate deflection shapes. Disc deflections are compared with test data and unbalance values are iterated in between Kalman Filter and Newmark Algorithm. The obtained unbalanced deflection shape for a fixed time and at Y direction is as in Figure 3.24.

For Kalman Filter inputs, the process noise covariance value is taken as 0.0001 mm; the measurement noise covariance value is taken as 0.0001 mm and the initial error covariance value is used as 1 mm. These values are displacement values and are important for the convergence of the Kalman Filter. These values were iterated before running the final Kalman Filter calculations.

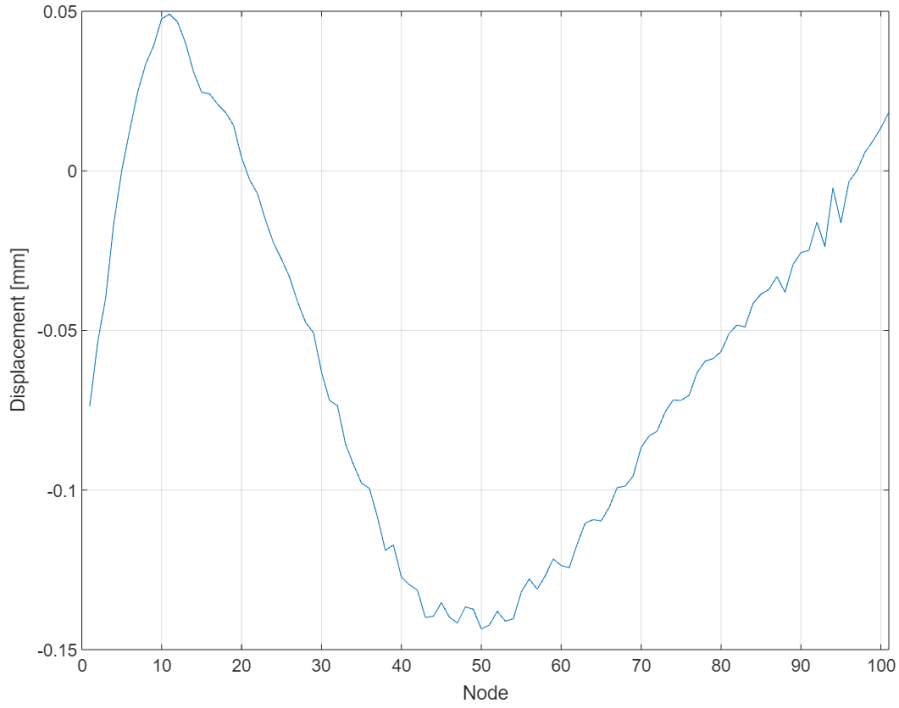

Figure 3.24: Shaft deflection at t=1.5625 s and Y direction.

Unknown displacements are generated with the usage of the Kalman Filter. Displacements at Y directions and at Disc locations are as shared in Figure 3.25. DoFs; 161, 241 and 301 have smooth curves as an output since these are measured locations. On the other hand, DoF 101 data is not smooth as this is an estimated location.

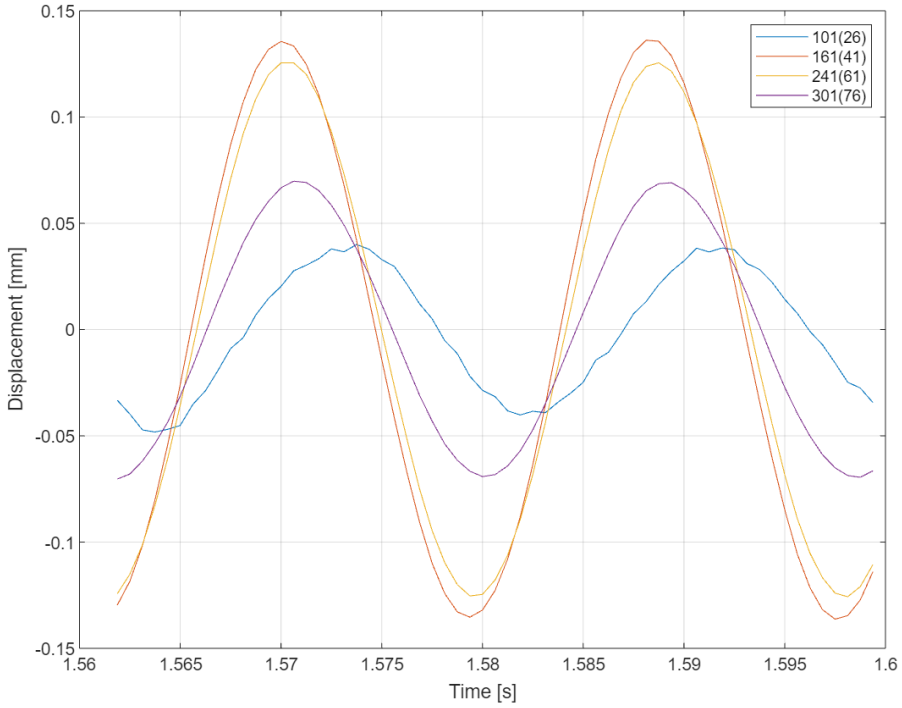

Figure 3.25: Disc displacements at Y direction obtained from Kalman Filter.

The next step is to generate the final unbalance values. Disc 1 unbalance value and its convergence plot are shared in Figure 3.26. Unbalance value is converged to 0.0086 kg.m for Disc 1.

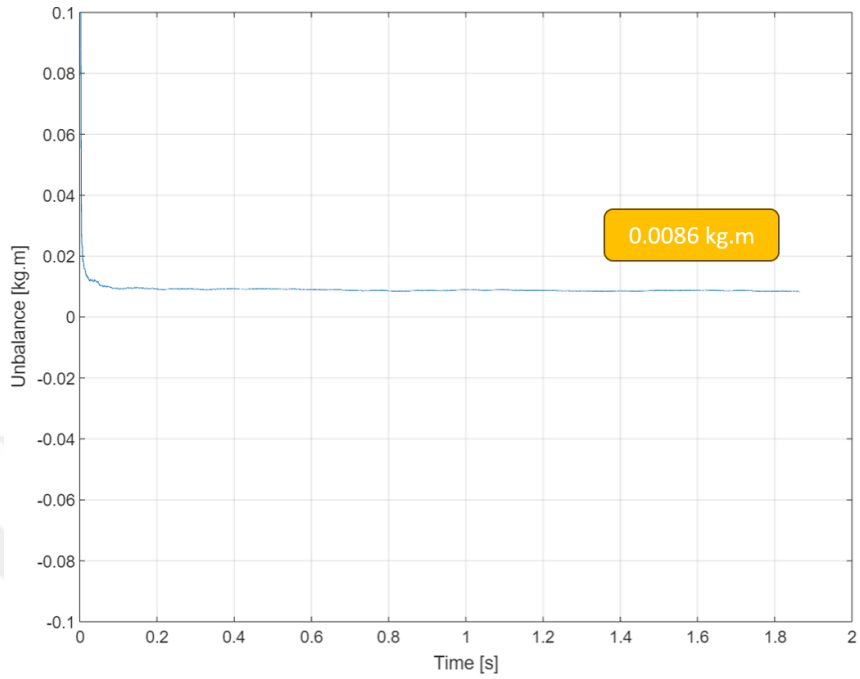

Figure 3.26: Disc 1 unbalance values obtained by Kalman Filter.

Disc 2 unbalance value plot is as in Figure 3.27. Unbalance value is converged to 0.0086 kg.m for Disc 2.

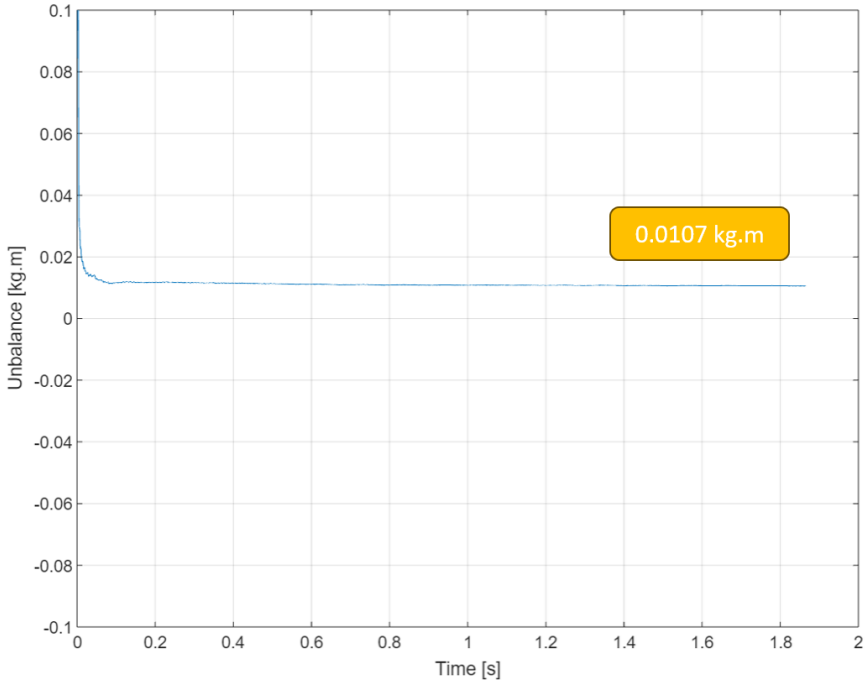

Figure 3.27: Disc 2 unbalance values obtained by Kalman Filter.

Disc 3 unbalance value plot can be seen in Figure 3.28. Unbalance value is converged to 0.0037 kg.m for Disc 3.

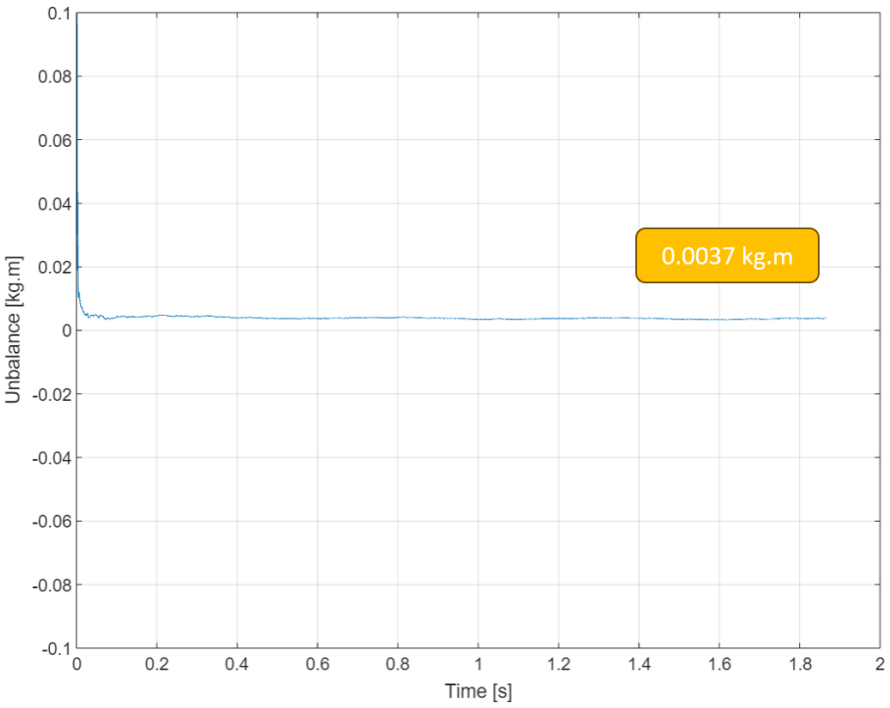

Figure 3.28: Disc 3 unbalance values obtained by Kalman Filter.

Disc 4 unbalance value plot is as in Figure 3.27. Unbalance value is converged to 0.00087 kg.m for Disc 4.

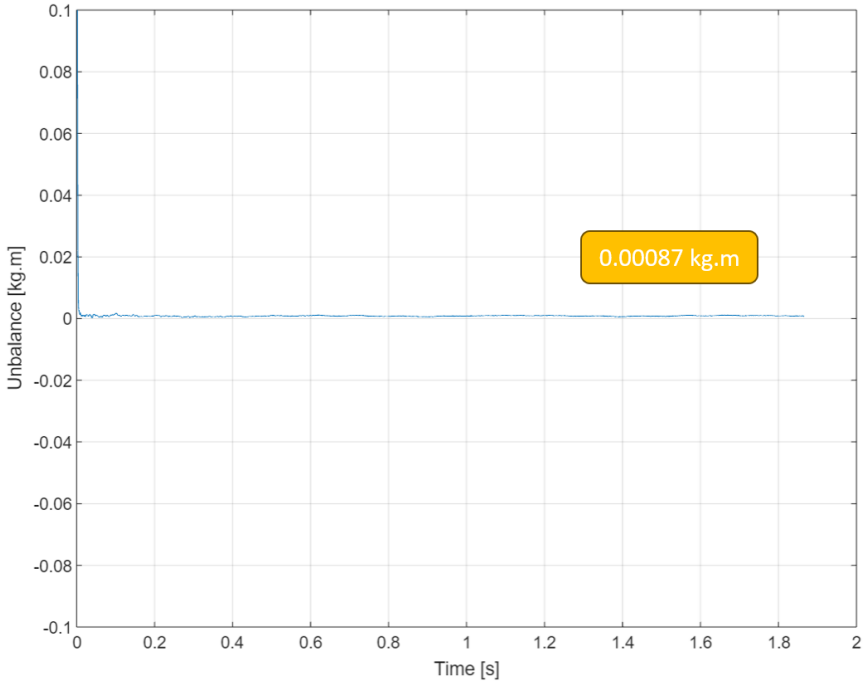

Figure 3.29: Disc 4 unbalance values obtained by Kalman Filter.

The phase angle of the unbalance direction is found to be 62°. It is important to note that these unbalance values and phase angle are induced values. Kalman Filter provides induced information that reflects the same physical outcomes as the real case.

3.2.5 Experimental results

Obtained unbalance values are applied as an external force to the Newmark Algorithm so that they act as balancing masses. After this process balanced shaft is obtained. Balanced shaft deflection shape is shared in Figure 3.30.

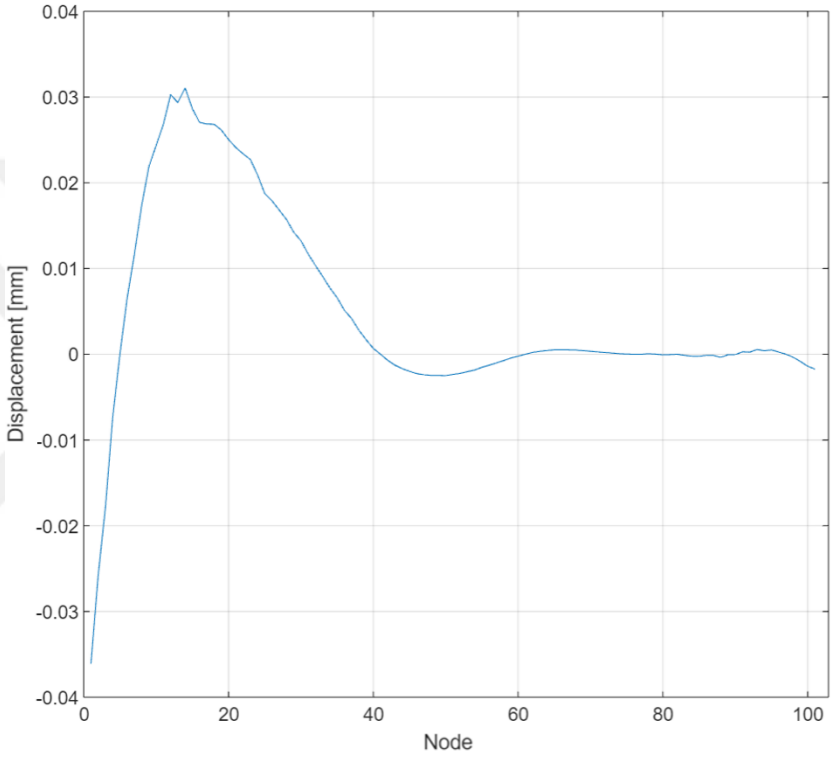

Figure 3.30: Balanced shaft deflection at t=1.5625 s and Y direction.

One can understand from Figure 3.30 that, nodes that have measured data available at disc locations; which are nodes 41, 61 and 76, have an accurate unbalance estimation as displacement on these locations is very low compared to the initial case. At node 21, whose displacements are generated by the Kalman Filter, the displacement value is increased, but it can be said that the overall maximum unbalance value is dropped from 0.05 mm to 0.03 mm.

To conclude; with this application, the shaft's first mode is balanced. Higher modes could not have been studied in this thesis as the data is not available suitable enough for the schedule.

4. CONCLUSIONS

The balancing approach, whose theory is described above, has a significant potential to accurately balance the rotating shafts.

First trials for the balancing procedure are made using simulation models, which are generated via MATLAB. During these trials, artificially added unbalance masses are used and system response is generated using a direct approach and with the help of the Newmark Algorithm, which is a numerical solver suitable for structural dynamics. Kalman Filter was able to generate the unbalance values with a reasonable margin.

Since the virtual problem defined above had been set up and solved using a direct approach only, overall unbalance values could be obtained instead of modal unbalances. In real cases; this could be worked only mode by mode, thus obtaining the real modal unbalance values.

One more important remark should be made for the covariance values, which were defined in Table 3.4. These values are directly determining the performance of the Kalman Filter. Normally, these are dependent on values such as sensor accuracy or system randomness. These should be investigated, worked and iterated for each real-life rotor balancing case.

After obtaining promising results with the virtual case, an experimental balancing is done. A test rig dedicated to balancing purposes is used. Displacement and rotational speed data are gathered from this test rig, which has a shaft and mounted discs on it. These values are used to run the Kalman Filter. Unbalance values and phase angles at those discs are obtained. Using the Newmark Algorithm, this scenario is regenerated virtually and validated by comparing obtained and test results. Balancing is carried out in this virtual case and promising results are obtained. This process is carried out for the first mode only due to the lack of higher modes' measurement data. The first mode's balancing is found to be promising, given the obtained results.

As the next step, obtained unbalance values should be put on the test rig as the unbalance masses and balancing quality should be checked. In case of acquiring successful results, higher modes shall be studied.

As described earlier, the balancing procedure proposed here uses a modal approach to set balancing conditions. So, when the modes are not well separated and two or more critical speeds are very close to each other, it will be very problematic to identify the modal unbalance values. This is a general problem related to all kinds of modal balancing approaches. Under these circumstances, a higher mode will be significantly contributing to the mode that is being measured for the time being and the desired mode isolation scenario will not take place.

Due to the usage of the Augmented Kalman Filter that targets the unbalance values directly, it could be possible to target whole unbalance values using transient data. Measurements could be made at speeds that are far enough from critical speeds. It should be restated that Kalman Filter is using a direct formulation. Initial trials using a model generated at MATLAB are promising for the time being but are yet to be studied further. If this approach is accurately possible, the complex balancing condition that is set using the modal approach could be abandoned and mode separation would be a problem no more.

REFERENCES

[1] **Adams, M. L.** (2010). *Rotating Machinery Vibration: From Analysis to Troubleshooting.* Boca Raton, FL: CRC Press.

[2] **Darlow, M.** (1989). *Balancing of High-Speed Machinery.* New York: Springer-Verlag.

[3] **Ehrich, F.** (1992). *Handbook of Rotordynamics.* Malabar: Krieger Publishing Company.

[4] **Fei, Z.-x., Tong, S.-g., & Wei, C.** (2013). Investigation of the dynamic characteristics of a dual rotor system and its start-up simulation based on finite element method. *Journal of Zhejiang University - Science A: Applied Physics & Engineering.* Hangzhou.

[5] **Ishida, Y., & Yamamoto, T.** (2012). *Linear and Nonlinear Rotordynamics A Modern Treatment with Applications.* Singapore: Wiley-VCH Verlag Gmbh & Co. KGaA.

[6] **Jiang, J., Luo, S., Mohamed, M. S., & Liang, Z.** (2020). Real-Time Identification of Dynamic Loads Using Inverse Solution and Kalman Filter. *MDPI Applied Sciences.*

[7] **Kramer, E.** (1993). *Dynamics of Rotors and Foundations.* Darmstadt: Springer-Verlag.

[8] **Krysl, P., & Endres, L.** (2005). Explicit Newmark/Verlet algorithm for time integration of the rotational dynamics of rigid bodies. *International Journal for Numerical Methods in Engineering.*

[9] **Lee, C.-W.** (1993). *Vibration Analysis of Rotors.* Springer Science+Business Media Dordrecht.

[10] **Liu, R., Dobriban, E., Hou, Z., & Qian, K.** (2021). Dynamic Load Identification for Mechanical Systems: A Review. *Archives of Computational Methods in Engineering.* Barcelona.

[11] **Lourens, E., Reynders, E., De Roeck, G., Degrande, G., & Lombaert, G.** (2011). An Augmented Kalman Filter for force identification in structural dynamics. *Mechanical SystemsandSignalProcessing.*

[12] **Matsushita, O., Tanaka, M., Kanki, H., Kobayashi, M., & Keogh, P.** (2017). *Vibrations of Rotating Machinery Volume 1. Basic Rotordynamics: Introduction to Practical Vibration Analysis.* Springer Japan.

[13] **Mereles, A., & Cavalca, K. L.** (2020). Mathematical modeling of continuous multi-stepped rotor-bearing systems. *Applied Mathematical Modelling.*

[14] **Mereles, A., & Cavalca, K. L.** (2021). Modeling of Multi-stepped Rotor-bearing Systems by the Continuous Segment Method. *Applied Mathematical Modelling.*

[15] **Niu, Y., Klinkov, M., & Fritzen, C.-P.** (2011). Online force reconstruction using an unknown-input Kalman filter approach. *International Conference on Structural Dynamics.* Leuven.

[16] **Sethu, R., Bhagat, A., Sujatha, C., & Narayanan, S.** (2015). Comparison of Various Techniques Used For Estimation of Input Force and Computation of Frequency Response Function (FRF) From Measured Response Data. *International Congress on Sound and Vibration.* Florence.

[17] **Shrivastava, A., & Mohanty, A. R.** (2020). Identification of unbalance in a rotor-bearing system using Kalman filter–based input estimation technique. *Journal of Vibration and Control.*

[18] **Turhan, Ö.** (2017). *Mekanik Titreşimler-I: Ayrık Lineer Sistemler.* Nobel.

[19] **Zou, D., Zhao, H., Liu, G., Ta, N., & Rao, Z.** (2019). Application of augmented Kalman filter to identify unbalance load of rotor-bearing system: Theory and experiment. *Journal of Sound and Vibration.*

CURRICULUM VITAE

Name Surname **:** Canberk Namık

EDUCATION **:**

- **B.Sc.** **:** 2020, Istanbul Technical University, Mechanical Engineering Faculty, Mechanical Engineering Department

PROFESSIONAL EXPERIENCE AND REWARDS:

- May 2021 – February 2023: BMC Power, MBD & NVH Analysis Engineer
- February 2023 – (Ongoing): GE Aerospace, Design Engineer-Mechanical Component